ANL-08/01

Argonne NATIONAL LABORATORY

# Initial Assessment of the Operability of the VHTR-HTSE Nuclear-Hydrogen Plant

Nuclear Engineering Division

**About Argonne National Laboratory**

Argonne is a U.S. Department of Energy laboratory managed by UChicago Argonne, LLC under contract DE-AC02-06CH11357. The Laboratory's main facility is outside Chicago, at 9700 South Cass Avenue, Argonne, Illinois 60439. For information about Argonne, see www.anl.gov.

**Availability of This Report**

This report is available, at no cost, at http://www.osti.gov/bridge. It is also available on paper to the U.S. Department of Energy and its contractors, for a processing fee, from:

U.S. Department of Energy
Office of Scientific and Technical Information
P.O. Box 62
Oak Ridge, TN 37831-0062
phone (865) 576-8401
fax (865) 576-5728
reports@adonis.osti.gov

ANL-08/01

# Initial Assessment of the Operability of the VHTR-HTSE Nuclear-Hydrogen Plant

by
R.B. Vilim
Nuclear Engineering Division, Argonne National Laboratory

September 2007

CONTENTS

LIST OF FIGURES

LIST OF TABLES

## ABSTRACT

The generation of hydrogen from nuclear power will need to compete on three fronts: production, operability, and safety to be viable in the energy marketplace of the future. This work addresses the operability of a coupled nuclear and hydrogen-generating plant while referring to other work for progress on production and safety. Operability is a measure of how well a plant can meet time-varying production demands while remaining within equipment limits. It can be characterized in terms of the physical processes that underlie operation of the plant. In this work these include the storage and transport of energy within components as represented by time constants and energy capacitances, the relationship of reactivity to temperature, and the coordination of heat generation and work production for a near-ideal gas working fluid. Criteria for assessing operability are developed and applied to the Very High Temperature Reactor coupled to the High Temperature Steam Electrolysis process, one of two DOE/INL reference plant concepts for hydrogen production.

Results of preliminary plant control and stability studies are described. A combination of inventory control in the VHTR plant and flow control in the HTSE plant proved effective for maintaining hot-side temperatures near constant during quasi-static change in hydrogen production rate. Near constant electrolyzer outlet temperature is achieved by varying electrolyzer cell area to control cell joule heating. It was found that rates of temperature change in the HTSE plant for a step change in hydrogen production rate are largely determined by the thermal characteristics of the electrolyzer. It's comparatively large thermal mass and the presence of recuperative heat exchangers result in a tight thermal coupling of HTSE components to the electrolyzer. It was found that thermal transients arising in the chemical plant are strongly damped at the reactor resulting in a stable combined plant. The large Doppler reactivity component, three times greater than next reactivity component, per unit temperature, is mainly responsible. This is the case even when one of the conditions for out-of-phase oscillations between reactor inlet and outlet temperature, a large time for transport of process heat between the reactor and chemical plant, exists.

# 1. INTRODUCTION

There are three performance-related aspects that must be addressed in studies aimed at commercialization of hydrogen generation using nuclear power. They are production, operability, and safety and their successful navigation will lead to a plant design that is viable in the commercial marketplace along with a set of Technical Specifications for operating the plant. Briefly, production is the task of obtaining hydrogen in an economical manner at full power operation. Operability is the ability to perform plant startup, load change, and shutdown without the need for complex control systems to maintain important process variables within limits. It also includes a measure of how stable the inherent response of the plant is during operational transients. Safety is the task of ensuring the plant can be shut down in a safe manner following an equipment failure or operator error. Engineering analyses are needed for assessing production, operability, and safety.

This report focuses on operability. Operability is a function of the inherent characteristics of the plant and, hence, can be shaped at the design stage. An important objective is to ensure that values of process variables during operation do not overly constrain plant life through excessive mechanical stress or creep. Operability is addressed in the course of setting the plant load schedule and the plant response to step changes in load. The load schedule specifies values of important plant process variables at each power level over the normal operating range. For the VHTR process variables that have strict limits are fuel and reactor structure temperatures and coolant pressures and temperatures in heat transport piping. The load schedule takes in startup and shutdown as well as normal load changes associated with changes in production demand. There will be separate load schedules for startup/shutdown and for production. The plant response to a step change in load demand gives the magnitude of the deviation in plant variables from steady state and the rate at which deviations die away. A change in demand can arise from either the grid (change in power from the dispatcher) or an anticipated upset that requires shutting down the plant. The goal again is to ensure operational life is not overly limited by excessive time rates of change. In part this is achieved by having deviations naturally die away. Otherwise the plant is unstable and ability to adhere to design load schedule for safe operation will be compromised.

The other two goals, those of production and safety, are being studied separately outside of this report. The HyPEP code [Oh et al. 2006] is being developed to address production in terms of efficiency and economics. Safety is to be examined in the future. This will involve determining the safety systems needed to maintain safe conditions following a failure of equipment or control systems.

The current work on operability is qualified here with respect to the future role of nuclear hydrogen in the national energy mix. The demand for electricity and/or hydrogen will place operational constraints on a particular plant. In an electricity-generating plant the product is not easily stored so operational flexibility to change power to meet varying electric grid demand must be provided. In a commercial nuclear power plant the production range needed is typically 25 to 100 percent of full power. In a chemical plant, however, the product can be more easily stored so there is not as great a need for partial power operation. The chemical plant typically runs at full power with short term variations in demand buffered by drawing from or adding to

stored chemical inventory. What is an appropriate goal for product output and mix for a nuclear-hydrogen plant (i.e. hydrogen only or co-generation) is outside the scope of this work and will need to be addressed in future systems integration work. The optimum mix depends on the future markets for hydrogen and electricity on a daily, seasonal, yearly, and geographic basis. In absence of this information it is assumed in this work that hydrogen is the sole product delivered at the plant fence. The appropriateness of this assumption depends on the outcome of future energy system studies.

In summary this report investigates the operability of a nuclear-hydrogen plant. A plant control strategy is developed and the load schedule and the step response are examined. Identification of important phenomena that shape the operational behavior of the plant guides the work.

# 2. METHODS

Operability is assessed by examining the behavior of the combined plant and control system for two types of operational maneuvers, a quasi-static change and a step change in hydrogen production rate. The process variable values are examined to see that they remain within limits set for normal operation which includes both absolute value and time rate of change value. The methods for identifying important phenomena and for characterizing the plant response are described in this section.

## 2.1 Time Scale of Phenomena

The combined plant response is shaped by the time constants of the various components. The time constants and where they appear in the flowpaths for the transport of conserved quantities can provide insight into the time behavior of the overall plant.

The time response of a component is in the neighborhood of an operating point given by the ordinary differential equation

$$\frac{d}{dt}y = \frac{-1}{\tau}\left[\, y + F\left[u(t)\right] \,\right] \tag{2-1}$$

where *u(t)* is the forcing function, *y* is the observed process variable, *F* is a function of *u*, and $\tau$ is the time constant. The role of the time constant is made evident by applying a step input to the component. The initial steady state satisfies from Eq. (2-1)

$$y\left(0^-\right) + F\left[u\left(0^-\right)\right] = 0\ , \tag{2-2}$$

so the component response for a step in *F* applied at *t=0* is

$$\frac{y(t) - y(\infty)}{y\left(0^-\right) - y(\infty)} = e^{\frac{-t}{\tau}}, \quad t > 0 \tag{2-3}$$

where *y(∞)* designates the new steady state. One sees that the observed variable moves to the new steady state with time constant $\tau$.

Analytic expressions for time constants and energy capacitances for the major components in a coupled VHTR and HTE plant are derived in this report.

## 2.2 Component Temperature Rates of Change

The plant operational behavior can be characterized to the first-order by the response to a step change in demand. Such changes may arise with the hydrogen distribution system or the electric grid. The time taken to come into equilibrium with the new demand condition, termed the *response time*, and the interim deviation compared to that if the change were carried out quasi-

statically, termed the *overshoot*, are important. The response time is important for meeting production goals while the overshoot is important for longevity-related integrity of structures.

Analyses based on component time constants and thermal capacitances can provide a measure of response time. Further, such analyses provide insight into what is controlling plant response and provide an adjunct to detailed transient simulation. The time constants and thermal capacitances control how long before the core and heat sink powers come back into equilibrium with each other after a change in conditions. A change in local conditions at the heat source (sink) flows through a series of processes each with a characteristic time constant before reaching the heat sink (source) where the temperature and flow changes create feedback effects that operate to bring all processes back to equilibrium. But until equilibrium is restored, a power generation imbalance gives rise to an energy imbalance approximated by

$$\delta E = \delta P \sum \tau_i \tag{2-4}$$

where $\delta P$ is an initial step change in power and the $\tau_i$ are a series of process time constants through which the change must propagate before feedback effects occur to bring heat sink and core power back into equilibrium. The change in temperature caused by this power imbalance averaged among the *i* processes is

$$\delta T = \frac{\delta P \sum \tau_i}{\sum \left(\rho V C_p\right)_i} \tag{2-5}$$

If the original and terminal plant states are on the normal plant operating curve, as is the case for the instances we will look at, then the overshoot in temperature is given by

$$\delta T_{os} = \frac{\delta P \sum \tau_i}{\sum \left(\rho V C_p\right)_i} - \delta T_{load} \tag{2-6}$$

where $\delta T_{load}$ is the change in temperature in going from the original to the new operating point on the plant operating curve or load schedule. To make use of the above expression, one first needs to identify the propagation path for the transient and to calculate the time constant and thermal capacitances of the processes along the propagation path.

The rate of change in temperature before equilibrium is reached is from Eq. (2-5)

$$\frac{d\delta T}{dt} = \frac{\delta P}{\sum \left(\rho V C_p\right)_i} . \tag{2-7}$$

## 2.3 Load Schedule

The full power operating point is set based on production goals while subject to material limits that include creep and thermal stress. Previous work [Oh 2006 and Oh 2007a] addressed the design of equipment for meeting these objectives. The simulation codes HYSYS and GAS-PASS [Vilim 2004] were used to calculate the full power condition and identified active control elements including pump, compressor, turbine, and electrolyzer needed.

In moving from designing for production (i.e. full power operation) on to designing for operability (i.e. partial power operation) the task is to specify how the outputs of these elements change with load. The specification must satisfy the material limits mentioned where thermal stresses may now include those brought about by time rates of change.

The partial power operating point is a continuum over power and is given by the *load schedule*. The load schedule specifies the value of each process variable as a function of plant power. Good operability as represented by reduced thermal stresses during power change is achieved by developing a load schedule that maintains temperature constant at the hottest points in the plant (e.g. reactor outlet) over power while at load. A mathematical relation shows what can be achieved from the standpoint of the number of independently controllable actuators needed to achieve constant temperature at a given number of points and the values actuator outputs need to assume.

Each of the components in the plant in the steady state satisfies an equation of the form

$$0 = [\, y + F\,[\underline{u}(t)]\,] \tag{2-8}$$

where

$\underline{u}(t)$ = vector of input forcing functions,
$F$ = function of $u(t)$,
$y$ = component output.

Assume for the sake of exposition that there are three control variables: two flowrates, $w_1$ and $w_2$, and rod reactivity, $\rho$. Coupling the equations for all components leads to a system of equations for the plant state vector expressed in terms of the control variables (assuming constant properties)

$$[T_1\, T_2 \ldots T_n]^T = A_o(w_1, w_2, \rho)^{-1}\, b_o(w_1, w_2, \rho) \tag{2-9}$$

where the $T_i$ are temperatures, $A_o$ is a matrix whose elements are functions of the control variables, and $b_o$ is a vector.

The control variables are written as linear functions of the plant power

$$w_1 = m_1 P + b_1$$
$$w_2 = m_2 P + b_2$$
$$\rho = m_3 \left( P - P_0 \right)$$

where $m_1$, $m_2$, $m_3$, $b_1$, and $b_2$ are constants.

Differentiating the above set of equations with respect to power gives a set of load schedule coefficients that defines the load schedule about an operating point

$$\left[ \frac{dT_1}{dP} \frac{dT_2}{dP} \bullet\bullet\bullet \frac{dT_n}{dP} \right]^T = A_1(m_1, m_2, m_3, T_1, T_2, ..., T_n)^{-1} b_1(m_1, m_2, m_3) \qquad (2\text{-}10)$$

One sees from the above equation that three load coefficients can be arbitrarily assigned through the three parameters $m_1$, $m_2$, and $m_3$. This expression holds at a particular power. It can be applied repeatedly at different power to achieve the load schedule desired for three temperatures. In general, assigning values to $n$ temperatures over the load range will require $n$ actuators.

It is apparent that a simulation code equipped with the proper features can be used to determine the output of each actuator as a function of load to achieve a desired load schedule. Essentially, for given values for the process variables on the left-hand side of Eq. (2-9) at a given power, the unknowns on the right-hand side are solved for. A load schedule is obtained by performing this calculation at each power. The GAS-PASS/H code has this capability.

## 2.4 Startup

The same concept of using actuators to manage temperatures also applies for design of the startup schedule. However, in any one component there may now be multiple physics regions that must be passed through one after the other. In the reactor, the core passes from being initially subcritical, then critical with delayed neutrons, and finally critical with delayed neutrons and temperature feedback. In a boiler the water is initially subcooled, then becomes saturated with unity quality at the exit, and finally possibly superheated at the exit. A condenser passes through analogous regions. A helium turbine may initially function as a compressor driven by the generator until temperatures and pressures reach the point where the turbine produces work.

Essentially a load schedule must be developed for each physics region the plant passes through during startup. Simulation of this requires model switching as each region is passed through. As a result calculation of plant startup is more complex. The need for model switching will need to be provided for in future simulations.

## 2.5 Stability Assessment

A stable combined plant is important for good operability. A physical system is stable if the transition to a new state, as driven by altered forcing function values, is marked by a smooth and non-oscillatory transition. Stability can be qualitatively assessed by examining the system response to a step change in an input variable. Since a step is composed of an infinite set of

frequencies it excites all modes of the system. The stability can also be assessed by more formal methods that examine eigenvalues of the system linearized about an operating point. [Depiante, 1994] The physical processes that govern the response of the reactor to a change in the load are described and a simple expression that predicts how reactor stability trends with plant parameter values is given below.

There is a natural tendency for reactor power to follow a change in heat sink load. An increase in load reduces heat sink outlet temperature which propagates to reduce reactor core inlet temperature, adding reactivity which increases power. The resulting core outlet temperature increase propagates back to the heat sink providing additional heat to meet the increase in power. The potential for oscillations arises if the heat sink does not attenuate this temperature front. In this case the front moves on to the core where it raises inlet temperature and causes reactor power to decrease. One sees that there is the potential for core power to alternately increase and decrease as the reactor inlet and outlet temperatures change out of phase with each other. The degree to which core power oscillations are dampened is a function of the attenuation of the temperature front at the heat sink and the size of the reactivity inlet temperature coefficient.

A simple reactivity balance shows how stability trends with integral reactivity parameters. The reactor power in the asymptote is related to the flowrate and inlet temperature through

$$0 = A\,(P - 1) + B\,(\frac{P}{W} - 1) + \mathrm{C}\,\delta T_i \tag{2-11}$$

as derived in Section 5.1.4. The change in reactor outlet temperature expressed as a function of change in reactor inlet temperature is then

$$\delta T_{out} = \left( 1 - \frac{C\,\Delta T_{c-100} / B}{\frac{A}{B} + 1} \right) \delta T_i \tag{2-12}$$

where $A$, $B$, and $C$ are integral reactivity parameters, $P$ and $W$ are normalized power and flow, respectively, and $\delta T_i$ is change in inlet temperature. If the expression within the parentheses is negative, then a change in inlet temperature in one direction leads to a change in outlet temperature in the opposite direction. Hence, to the extent the heat sink passes through without attenuation a primary hot leg temperature front associated with an increase in reactor power due to an initial reactivity addition, the reactor power will begin to decrease on negative temperature reactivity a time later equal to the propagation time around the primary system. For oscillations to occur, this time must be long enough that the initial reactor power increase (due to the original reactivity addition) begins to equilibrate before the temperature front makes it back to the reactor. Thus, oscillations are favored if 1) the heat sink weakly attenuates primary hot leg temperature fronts, 2) the loop propagation time is more than a few tens of seconds (making it greater than the core time constant), and 3) the expression in parentheses in Eq. (2-12) is negative. The amplitude of these oscillations will increase as $C\Delta T_{c-100} / B$ becomes a larger positive number and $A/B$ a smaller positive number provided the ratio of the two is more than unity.

# 3. MODELS

Models for the dynamic behavior of system components are developed by writing the conservation balances in lumped parameter form. The resulting ordinary differential equations have been programmed in the GAS-PASS/H code where they are solved numerically to obtain a time-dependent solution. The ordinary differential equations are also linearized to obtain expressions for the time constant and energy capacitance of a component.

## 3.1 Electrolyzer

The electrolytic cell modeled has a planar rectangular geometry consisting of the following components. Listed from cell exterior and moving through the cell in a line normal to the cell plane to the opposite side we have: steel separator, edge rails, porous cathode, electrolyte, porous anode, edge rails, and separator. The two inlet streams enter at right angles to each other with each stream entering along the normal to a cell edge. Of these components only the electrodes and electrolyte are in close contact with the gas streams and are sites of significant energy deposition/generation.

In modeling the cell note that the electrochemical processes reach equilibrium at a much faster rate than the thermal processes. It is reasonable then to model them as quasi-static. It is assumed that the two flow streams entering the cell do so at the same temperature. It is also assumed that the two flow streams within the interior of the cell are perfectly mixed and that each stream exits the cell at the same temperature. Further, the cell components listed above are all assumed to be in thermal equilibrium with each other and with the flow streams within the cell. Then an energy balance on the cell gives for the rate of change of cell temperature

$$\left[\left(\rho V C_p\right)_s + \left(\rho V C_v\right)_g\right] \frac{d}{dt} T =$$
$$\left[\begin{array}{c} m_{H_2O-i-cath}\, h_{H_2O}\left(T_i,P\right) + m_{H_2-i-cath}\, h_{H_2}\left(T_i,P\right) + m_{N_2-i-cath}\, h_{N_2}\left(T_i,P\right) + \\ m_{O_2-i-anode}\, h_{O_2}\left(T_i,P\right) + m_{N_2-i-anode}\, h_{N_2}\left(T_i,P\right) \end{array}\right] -$$
$$\left[\begin{array}{c} m_{H_2O-o-cath}\, h_{H_2O}\left(T,P\right) + m_{H_2-o-cath}\, h_{H_2}\left(T,P\right) + m_{N_2-o-cath}\, h_{N_2}\left(T,P\right) + \\ m_{O_2-o-anode}\, h_{O_2}\left(T,P\right) + m_{N_2-o-anode}\, h_{N_2}\left(T,P\right) \end{array}\right] + \tag{3-1}$$
$$Q + W$$

where

| | | |
|---|---|---|
| $\rho$ | = | density, |
| $V$ | = | volume, |
| $T$ | = | temperature, |
| $m$ | = | species mass flow rate (kg/s), |
| $h$ | = | specific enthalpy (joules/kg), |
| $Q$ | = | rate of heat transfer to the electrolyzer, |
| $W$ | = | rate of electrical work supplied to the electrolyzer, and |
| P | = | pressure, |

and where subscripts *i* and *o* represent inlet and outlet, respectively, and *s* and *g* represent structure and gas, respectively. The electrical work is

$$W = V_{cell} \cdot A \cdot i \tag{3-2}$$

$$W = V_{cell} \cdot A \cdot \left( \frac{V_{cell} - V_N}{ASR} \right) \tag{3-3}$$

where

| | | |
|---|---|---|
| $V_{cell}$ | = | voltage applied to cell, |
| $i$ | = | current density, |
| $A$ | = | electrolyte area, and |
| $ASR$ | = | area specific resistance, |

and where

$$V_N = \frac{-1}{2F} \left[ \Delta G_f{}^0(T) + RT \ln \left[ \left( \frac{f_{H_2} \, f_{O_2}{}^{\frac{1}{2}}}{f_{H_2O}} \right) \left( \frac{P}{P_{STD}} \right)^{\frac{1}{2}} \right] \right] \quad \text{and} \tag{3-4}$$

$$ASR = \left( ASR \right)_0 + C_1 \exp\left( \frac{C_2}{T} \right) \tag{3-5}$$

where *C1* and *C2* are constants and *T* is in degrees K.

The characteristic times for how cell output quantities (species concentration, structure temperatures, and temperatures of gas streams) respond to changes in cell inlet conditions (current and inlet temperature) are derived for several simplifying and reasonable assumptions. The species concentrations and the gas stream temperatures respond much more quickly to changes in cell inlet conditions than do the temperatures of structures. These elements can be treated quasi-statically compared to the structures. Further, of the structures only the electrodes and electrolytes are in intimate contact with the changing thermal conditions in the cell. Assume that only water enters the cell and that only hydrogen and oxygen exit the cell. The heat capacity of the gas inside the cell is negligible and it is assumed the cell is operated adiabatically. Then from Eq. (3-1)

$$\rho V C_p \frac{d}{dt} T = m_{H_2O} \; h_{H_2O} - \left( m_{H_2} h_{H_2} + m_{O_2} h_{O_2} \right) + W \tag{3-6}$$

$$m_{H_2} = \frac{A_{H_2}}{A_{H_2O}} m_{H_2O} \qquad m_{o_2} = \frac{A_{O_2}}{2 A_{H_2O}} m_{H_2O} \tag{3-7}$$

$$\rho V C_p \frac{d}{dt} T = m_{H_2O}\left[ h_{H_2O}(T_i) - \frac{1}{A_{H_2O}}\left( A_{H_2} h_{H_2}(T) + \frac{A_{0_2}}{2}(T) \right) \right] + W \tag{3-8}$$

where $\rho$ is the density and $V$ is the volume and $T$ is temperature of the electrodes and electrolyte (i.e. thermally active structures), $m$ is species mass flow rate (kg/s), $h$ is specific enthalpy (joules/kg), $W$ is rate of electrical work supplied to the electrolyzer, $A$ is atomic number, and subscript $i$ represents inlet.

Suppose control on $i$ (i.e. $m_{H2}$) and accept $V_{cell}$

$$m_{H_2O} = \frac{A_{H_2O} A}{2F} \tag{3-9}$$

Writing the electrical work in terms of current, $i$, Nernst voltage, $V_N$, cell area, $A$, and area specific resistance, $ASR$,

$$\begin{aligned} W &= V_{cell}\ A\ i \\ &= \left(V_N + i \cdot ASR\right) A\ i \\ &= A V_N\ i + A \cdot ASR\ i^2 \\ &= A V_N(T)\ i + A \cdot ASR\ i^2 \end{aligned} \tag{3-10}$$

$$\begin{aligned} \rho V C_p \frac{d}{dt} T = \frac{A_{H_2O} A}{2F}\ i \left[ h_{H_2O}(T_i) - \frac{1}{A_{H_2O}} \left( A_{H_2}\ h_{H_2}(T) + \frac{A_{O_2}}{2} h_{O_2}(T) \right) \right] \\ +\ A V_N(T)\ i + A \cdot ASR\ i^2 \end{aligned} \tag{3-11}$$

and then linearizing the equation

$$\begin{aligned} \rho V C_p \frac{d}{dt} \delta T = \frac{A_{H_2O} A}{2F}\ \left[ i_o\ C_{\rho_{H_2O}} \delta T_i + h_{H_2O}(T_{i_o}) \delta i \right] \\ - \frac{A A_{H_2}}{2F} \left[ i_o\ C_{\rho_{H_2}}\ \delta T + h_{H_2}(T_o) \delta i \right] \\ - \frac{A A_{O_2}}{4F} \left[ i_o\ C_{\rho_{O_2}}\ \delta T + h_{O_2}(T_o) \delta i \right] \\ + A \left[ i_o \frac{\partial V_N(T)}{\partial T} \delta T + V_N(T_o) \delta i \right] \\ + A \left[ ASR_o \left( i_o^2 + 2 i_o \delta i + (\delta i)^2 \right) + i_o^2 \frac{\partial}{\partial T} ASR\ \delta T \right] \end{aligned} \tag{3-12}$$

where subscript *o* represents the linearization point. The above equation gives the change in cell temperature (electrodes, electrolyte, and outlet gas streams) in terms of changes in cell current and temperature of the inlet gas streams. Collecting terms gives

$$\rho V C_\rho \frac{d}{dt}\delta T = \frac{-i_o A}{2F}\left[ A_{H_2} C_{\rho_{H_2}} + A_{O_2} C_{\rho_{O_2}} - 2F \frac{\partial V_N(T)}{\partial T} - 2F\ i_o \frac{\partial ASR}{\partial T} \right]\delta T$$
$$+ \frac{A}{2F}\left[ A_{H_2O}\ h_{H_2O}(T_{i_o}) - A_{H_2} h_{H_2}(T_o) - \frac{A_{O_2}}{2} h_{O_2}(T_o) + 2F\ V_N(T_o) + 4F \cdot ASR\ i_o \right]\delta i$$
$$+ \left[ \frac{A_{H_2O} A}{2F}\ i_o\ C_{\rho_{H_2O}} \right]\delta T_i \qquad (3\text{-}13)$$

and from the above according to Eq. (2-1) the cell time constant is

$$\tau^{-1} = \frac{i_o A}{2F(\rho V C_\rho)_s}\left[ A_{H_2}\ C_{\rho_{H_2}} + A_{O_2}\ C_{\rho_{O_2}} - 2F\ \partial\frac{V_{N(T)}}{\partial T} - 2F\ i_o \frac{\partial}{\partial T} ASR \right] \qquad (3\text{-}14)$$

where the various terms in this equation are given by

$$V_N = +\frac{1}{2F}\left[ \Delta G_f^o(T) + RT\ ln\left\{ \left( \frac{f_{H_2} f_{o_2}^{1/2}}{f_{H_2O}} \right)\left( \frac{P}{P_{STD}} \right)^{1/2} \right\} \right] \qquad (3\text{-}15)$$

$$\partial\frac{V_N}{\partial T} = +\frac{1}{2F}\left[ \frac{\partial \Delta G_f^o}{\partial T} + R\ ln\left\{ \left( \frac{f_{H_2} f_{o_2}^{1/2}}{f_{H_2O}} \right)\left( \frac{P}{P_{STD}} \right)^{1/2} \right\} \right] \qquad (3\text{-}16)$$

$$ASR = ASR_o + C_1\ exp\left( \frac{C_2}{T} \right) \qquad (3\text{-}17)$$

$$\partial\frac{ASR}{\partial T} = -\frac{C_1 C_2}{T^2}\ exp\left( \frac{C_2}{T} \right) = -\frac{C_2}{T}(ASR). \qquad (3\text{-}18)$$

## 3.2 Heat Exchanger

The efficiency of the closed Brayton cycle is very sensitive to pressure losses and so there is an incentive to use heat exchangers with a high effectiveness/low pressure drop characteristics. Generally, this implies plate and fin or printed circuit heat exchangers (PCHE) in a counter flow configuration. This section develops models for the PCHE.

The construction of a typical PCHE is shown in Figure 3-1. The design consists of alternating hot and cold plates with semi-circular parallel flow channels etched into the lower face of each plate with the channels carrying the respective hot and cold streams. The hot and cold streams flow in opposite directions.

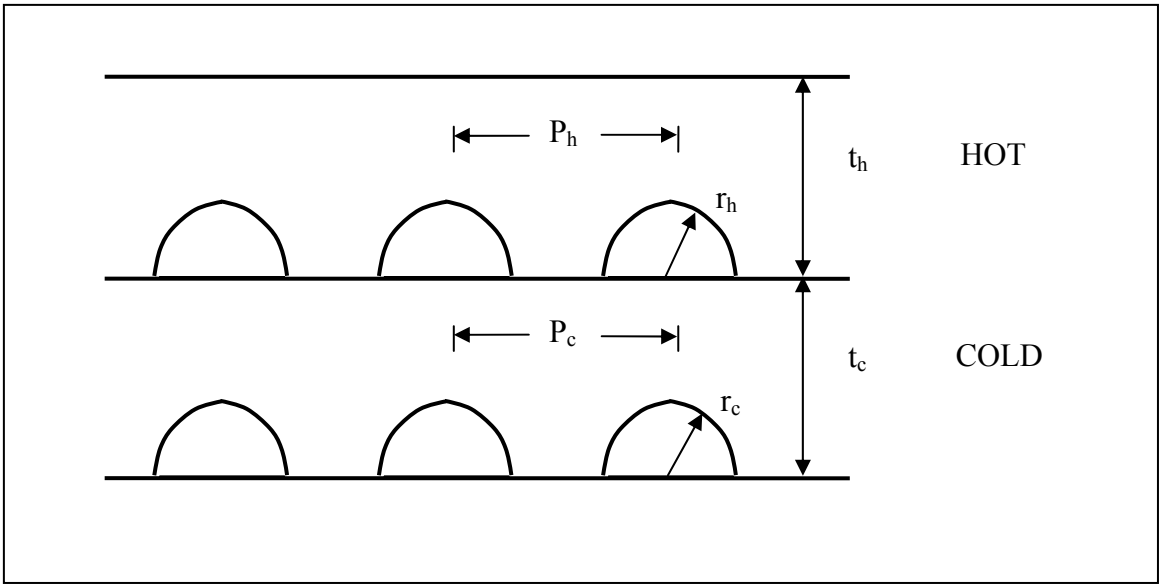


Figure 3-1 View of Printed Circuit Heat Exchanger in Cross Section

The energy equation for the hot side coolant node is

$$V\frac{d(\rho h)_{h_o}}{dt} = -Q_{h-t} + w_{h_i}h(T,P)_{h_i} - w_{h_o}h(T,P)_{h_o} \tag{3-19}$$

where $Q_{h\text{-}t}$ is the rate of total heat transfer from the hot side coolant to the heat transfer media which we refer to as a tube and $h$ is enthalpy. Similarly, the energy equation for the cold side coolant is

$$V\frac{d(\rho h)_{c_o}}{dt} = Q_{t-c} + w_{c_i}h(T,P)_{c_i} - w_{c_o}h(T,P)_{c_o} \tag{3-20}$$

where $Q_{t\text{-}c}$ is the rate of total heat transfer from the tube to the cold side coolant. The energy equation for the tube is

$$V\frac{d(\rho C_p T)_t}{dt} = -Q_{t-c} + Q_{h-t}. \tag{3-21}$$

In the case where the tube metal is lumped with one of the coolants rather than solving separately for its temperature, the heat transfer rate from hot to cold fluid is for constant fluid properties

$$Q = AU \frac{(T_{ho} - T_{ci}) - (T_{hi} - T_{co})}{\ln((T_{ho} - T_{ci})/(T_{hi} - T_{co}))}. \tag{3-22}$$

A unit cell delineated by four boundaries across each of which there is zero net energy flow is defined for characterizing the different heat transfer processes. Figure 3-2 shows two adjacent unit cells contained in the cross section of an infinite array of alternating hot and cold plates. We consider the upper unit cell in Figure 3-2. Both unit cells are similar enough that this one suffices for obtaining representative time constants. Heat flows from the hot channel on the bottom to the cold channel on the top. The dashed horizontal lines drawn through each channel identify cell boundaries across which there is not net flow of energy. Of course, the energy flow in the cell shown is two dimensional and it is assumed this distribution is known so that the cell boundaries can be drawn as the dashed lines shown. This establishes dimension *t'* shown in the figure.

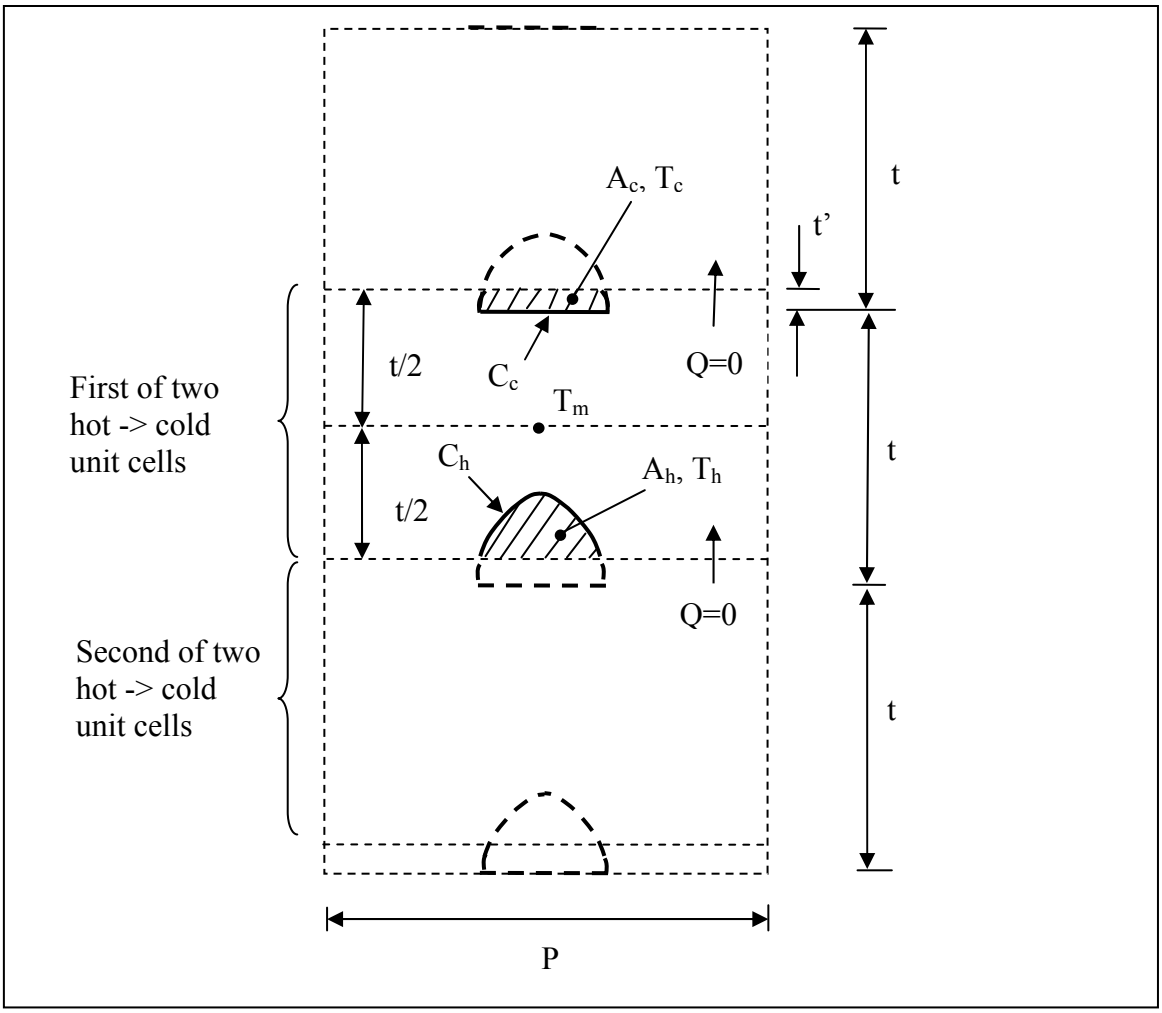


Figure 3-2 Unit Cells Defined for Infinite Array of Hot and Cold Channels

A one-dimensional representation of heat flow between the channels in the top unit cell is shown in Figure 3-2. This is of course an approximation to a multidimensional heat flow problem but captures to the first order the energy storage mechanisms and heat flow resistances of the three regions: the hot channel, the cold channel, and the intervening heat transfer media. The coolant in the channels that interacts with the heat transfer media in the cell is marked by the hash lines in the channels. This fluid has a cross sectional area denoted by $A$ and it makes contact with the media through circumference $C$. The circumference is the solid line that abuts the hash lines. The hot stream, media, and cold stream have average temperatures $T_h$, $T_m$, and $T_c$, respectively, shown in Figure 3-2. The heat transfer between the hot stream and the media is approximated by

$$T_h - T_1 = \frac{Q/l}{C_h h_h} \tag{3-24}$$

where $T_1$ is the temperature at the surface of the media in contact with the hot stream, $h_h$ is the heat transfer coefficient between the hot stream and the surface of the media, and $k$ is the thermal conductivity of the media. Similarly, the heat transfer through the media is approximated by

$$T_1 - T_m = \frac{Q/l}{\frac{kP}{t/2}\,\frac{(t/2*P - A_h)}{t/2*P}} \tag{3-25}$$

where $A_h$ is the hot fluid cross sectional area of the unit cell. The factor on the right in the denominator attempts to correct for the reduction in the cross section of the media caused by the hot channel and its subsequent effect on average conductivity. Alternatively, this correction factor could be obtained from the solution to the two-dimensional conduction equation for the media. The above two equations yield

$$Q = \bar{h}_{h-m}\, l\, (T_h - T_m) \tag{3-26}$$

where

$$\bar{h}_{h-m} = \left( \frac{1}{C_h h_h} + \frac{1}{\frac{kP}{t/2}\,\frac{(t/2*P - A_h)}{t/2*P}} \right)^{-1} . \tag{3-27}$$

Similarly, the heat flow between the media and the cold channel is given by

$$Q = \bar{h}_{m-c}\, l\, (T_m - T_c) \tag{3-28}$$

where

$$\bar{h}_{m-c} = \left( \frac{1}{C_c h_c} + \frac{1}{\frac{k\,P}{t/2}\,\frac{(t/2*P - A_c)}{t/2*P}} \right)^{-1} \quad . \tag{3-29}$$

An energy balance on the hot channel coolant in thermal contact with media over a length *l* gives

$$(\rho A l C_v)_h \frac{dT_h}{dt} = -(C_p w)_h (T_h - T_i) - \bar{h}_{h-m}\, l\, (T_h - T_m) \tag{3-30}$$

where $\rho$ is density, $C_p$ is specific heat, $w$ is flow rate, and subscript $i$ refers to inlet. Similarly, for the media

$$(\rho A l C_p)_m \frac{dT_m}{dt} = -\bar{h}_{h-m}\, l\, (T_m - T_h) - \bar{h}_{m-c}\, l\, (T_m - T_c). \tag{3-31}$$

Rewriting these two equations in terms of time constants,

$$\frac{dT_h}{dt} = -\frac{1}{\tau_{i-h}}(T_h - T_i) - \frac{1}{\tau_{h-m}}(T_h - T_m) \tag{3-32}$$

and

$$\frac{dT_m}{dt} = -\frac{1}{\tau_{m-h}}(T_m - T_h) - \frac{1}{\tau_{m-c}}(T_m - T_c) \tag{3-33}$$

where

$$\tau_{i-h} = \frac{(\rho A l C_v)_h}{(C_p w)_h}, \qquad \tau_{h-m} = \frac{(\rho A C_v)_h}{\bar{h}_{h-m}}, \qquad \text{and} \tag{3-34}$$

$$\tau_{m-h} = \frac{(\rho A C_p)_m}{\bar{h}_{h-m}}, \qquad \tau_{m-c} = \frac{(\rho A C_p)_m}{\bar{h}_{m-c}}. \tag{3-35}$$

Three nodes representing the hot side coolant, heat transfer media, and cold side coolant. A lumped parameter energy storage equation is written for each of the nodes. When writing these equations it is assumed from the standpoint of energy storage that there is perfect mixing of the energy that enters a node so that the node is at a uniform temperature.

General expressions are developed for the parameters $C_h$, $A_h$, $C_c$, and $A_c$ that appear above. The location of the zero heat flow boundaries in Figure 3-2 is referenced in terms of the displacement *t'*. In the absence of a solution to the two-dimensional conduction equation, we assume the zero net heat flow line is located where one-half of the channel perimeter lies above the line and the

other half below. The total channel perimeter is *r*(π+2)*. Let the angle between the base of the semi-circle and the radius that intersects the zero heat flow line be $\theta$. Then $\theta$ satisfies

$$\frac{1}{2}C = \frac{1}{2}r(\pi+2) = 2r + 2r\theta \quad \text{or} \qquad \theta = \frac{1}{4}(\pi - 2) \tag{3-36}$$

where $C$ is the total perimeter of the channel. We have then for the hot channel in the unit cell (i.e. hashed region) of Figure 3-2

$$C_h = r\left(\frac{\pi}{2}+1\right) \quad , \quad A_h = r^2\left(\frac{\pi}{2} - \theta - \sin\theta\cos\theta\right) \text{, and} \quad A_m = P\frac{t}{2} - A_h \tag{3-37}$$

where θ is given by Eq. (3-36). For the cold channel

$$C_c = C_h \qquad \text{and} \qquad A_c = \frac{\pi}{2}r^2 - A_h \tag{3-38}$$

## 3.3 Boiler

The response of the two-phase mixture temperature in a counterflow heat exchanger to changes in boundary conditions is derived. It is assumed the hot side is single phase liquid and that the cold side has saturated liquid water entering and saturated steam exiting. If we assume the water is on the shell side, then the energy equation for the water is

$$\frac{d}{dt}M_{H_2O}\, i \; + \; \left(\rho V C_p\right)_{shell}\frac{d}{dt}T_{sat} = Q + w_{fw}h_{fw} - w_s h_g \; . \tag{3-39}$$

The above equation lumps the heat capacity of the shell in with the water mixture.

If we assume no change in mass so that the feedwater flow equals steam flow, then

$$\frac{d}{dt}M_{H_2O} = 0 = w_{fw} w_s \, , \tag{3-40}$$

and Eq. (3-39) becomes

$$\frac{di}{dt} + \frac{\left(\rho V\, C_p\right)_{shell}}{M_{H_2O}}\frac{d}{dt}T_{sat} = \frac{1}{M_{H_2O}}\left[Q - w_{fw}\left(h_g - h_{fw}\right)\right] . \tag{3-41}$$

The first term in Eq. (3-41) can be expanded into

$$\frac{d}{dt}i = c\frac{dT_{sat}}{dt} + i_{fg}\frac{d}{dt}x \tag{3-42}$$

where

$$c = \left(1 - x\right)\frac{d}{dT} i_f + x\frac{d}{dt} i_g \ . \tag{3-43}$$

Then Eq. (3-41) becomes

$$\left[c + \frac{\left(\rho V C_\rho\right)_{shell}}{M_{H_2O}}\right]\frac{d}{dt} T_{sat} + i_{fg}\frac{d}{dt} x = \frac{1}{M_{H_2O}}\left[Q - w_{fw}\left(h_g - h_{fw}\right)\right]. \tag{3-44}$$

The derivative of the quality with respect to time in this equation is eliminated next.

Writing the conservation of volume equation for the mixture

$$M_{H_2O}\frac{d}{dt} v = 0 \ , \tag{3-45}$$

where we have made use of Eq. (3-40). Expanding Eq. (3-45) leads to

$$0 = \phi\frac{d}{dt} T_{sat} + v_{fg}\frac{d}{dt} x \ , \tag{3-46}$$

where

$$\phi = x\frac{d}{dT} v_g + \left(1 - x\right)\frac{d}{dT} v_f \ . \tag{3-47}$$

The equation for the saturation temperature is obtained by combining Eqs. (3-44) and (3-46) which gives

$$\frac{d}{dt} T_{sat} = \frac{1}{M\left[c + \dfrac{\left(\rho V C_p\right)_{shell}}{M} - \dfrac{\phi\, i_{fg}}{v_{fg}}\right]}\left[Q - w_{fw}\left(h_g - h_{fw}\right)\right]. \tag{3-48}$$

If the change in $T_{SAT}$ is small, then one can solve Eq. (3-48) with the properties and quality taken to be constant.

An expression for the heat transfer rate, $Q$, is obtained by assuming that the coolant axial temperature profiles are those that would result in the steady state given the instantaneous values of the boundary conditions. Then the log mean temperature model gives

$$\frac{T_{hi}-T_{sat}}{T_{ho}-T_{sat}} = exp\left[\frac{UA}{\left(wC_p\right)_h}\right] = K^{-1} \ . \tag{3-49}$$

and

$$Q = UA\,\frac{\left(T_{ho}-T_{sat}\right)-\left(T_{hi}-T_{sat}\right)}{\ln\left(\left(T_{ho}-T_{sat}\right)/\left(T_{hi}-T_{sat}\right)\right)} \tag{3-50}$$

where the subscript *h* refers to the hot side, *i* to the inlet, and *o* to the outlet. Using the above equation and neglecting the thermal inertia of the hot side coolant, a hot side energy balance gives

$$Q = \left(w\ C_p\right)_h \left(1-K\right)\left(T_{hi}-T_{sat}\right) . \tag{3-51}$$

The final equation for the saturation temperature in terms of the time dependent boundary conditions of hot side inlet temperature, feedwater enthalpy, and steam flowrate is obtained by substituting Eq. (3-50) into Eq. (3-48) which gives,

$$\frac{d}{dt}T_{sat} = \frac{-1}{\tau}\left[T_{sat} + F\left(t\right)\right] \ , \tag{3-52}$$

where

$$\frac{1}{\tau} = \frac{\left(wC_p\right)_h\left(1-K\right)}{M_{H_2O}\left[c + \dfrac{\left(\rho V C_\rho\right)_{shell}}{M_{H_2O}} - \dfrac{\phi\, i_{fg}}{v_{vg}}\right]} \ . \tag{3-53}$$

## 3.4 Reactor Core

This section describes the model developed for the reactor core and its application for simulating the response of the core to temperature perturbations that originate in the hydrogen plant.

### 3.4.1 Temperatures

The reactor core is a collection of fueled hexagonal columns with each column having axial coolant holes that connect the inlet plenum to the outlet plenum. The distribution of coolant flow among the columns is influenced by the presence of leakage paths between adjacent columns. A detailed prediction of the distribution of coolant is the subject of other work. [Vilim 2007a] In the present work we note that the flow of coolant is predominantly axially through the column holes. Then a one-dimensional representation of the core provides the main dependence of core temperatures on coolant inlet temperature and flowrate.

An averaged thermal-hydraulic behavior of the graphite column with its array of coolant holes and fuel holes is obtained by transforming into a unit cell annular geometry. This cell is shown in Figure 3-3. The radii of the three regions in the annular model are selected to preserve the areas in the original fuel element matrix and the number of unit cells is set equal to the number of coolant holes so that

$$n_{cl}\ A_{cl} = n_{cl}\ \pi(r_{cl}^{\ 2} - r_{gr}^{\ 2}) \qquad n_{cl}\ A_{gr} = n_{cl}\ \pi(r_{gr}^{\ 2} - r_{f}^{\ 2}) \qquad n_{cl}\ A_{f} = n_{cl}\pi r_{f}^{\ 2} \tag{3-54}$$

where the left-hand side of each equation is the area in the original fuel element and the right side is an equal area distributed across a number of unit cells (i.e. annular fuel elements) equal to the number of coolant channels. Here

| | | |
|---|---|---|
| *A* | = | cross-sectional area in the original fuel element on a per unit cell basis, |
| *n* | = | number of holes in the original fuel element, and |
| *r* | = | equivalent outer radius for annular pin representation |

and *f*, *gr*, *cl* represent fuel, graphite, and coolant, respectively. This transformation yields an effective one-dimensional conduction distance for the graphite.

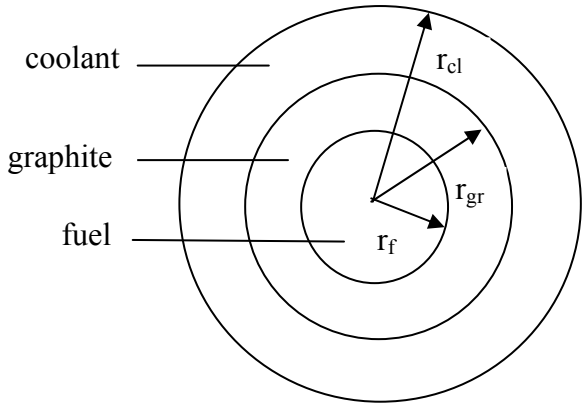


Figure 3-3 Transformed Fuel Element Geometry

Adopting this annular geometry the energy equation for the fuel in contact with the graphite is

$$(\rho C_p)_f \frac{dT_f}{dt} = Q_f - \frac{h_{f-gr} 2\pi r_f}{A_f}(T_f - T_{gr}) \tag{3-55}$$

where

| | | |
|---|---|---|
| $T_f$ | = | fuel temperature, |
| $Q_f$ | = | volumetric heat generation rate, |
| $h_{f\text{-}gr}$ | = | fuel to graphite heat transfer coefficient, |

$r_f$ = radius of fuel,
$A_f$ = cross sectional area of fuel, and
$T_{gr}$ = graphite temperature.

An expression for the heat transfer coefficient is obtained as follows. The analytic solution to the steady-state one-dimensional heat conduction problem gives the heat flux at the graphite-fuel interface as one-half of the graphite and fuel temperature rise times the heat transfer coefficient

$$\frac{1}{h_{f-gr}} = \frac{r_f}{4k_f} + \frac{\Delta r_{gr}}{2k_{gr}} + \frac{1}{h_{gap}} \tag{3-56}$$

where

$k_f$ = fuel conductivity,
$\Delta r_{gr}$ = graphite thickness, and
$h_{gap}$ = gap conductivity.

But one-half the graphite and fuel temperature rise is approximately the difference between the average fuel and average graphite temperature, $T_f - T_{gr}$. Thus, the heat transfer coefficient given above will result in Eq. (3-55) being very nearly satisfied at steady state.

The energy equation for the graphite is

$$(\rho C_p)_{gr} \frac{dT_{gr}}{dt} = \frac{h_{f-gr} 2\pi r_f}{A_{gr}} (T_f - T_{gr}) - \frac{h_{gr\text{-}cl} 2\pi r_{gr}}{A_{gr}} (T_{gr} - T_{cl}) \tag{3-57}$$

where

$T_{cl}$ = coolant temperature,
$h_{gr\text{-}cl}$ = cladding to coolant heat transfer coefficient,
$r_{gr}$ = outer radius of graphite, and
$A_{gr}$ = cross sectional area of graphite.

The graphite to coolant heat transfer coefficient is given by

$$\frac{1}{h_{gr\text{-}cl}} = \frac{\Delta r_{gr}}{2k_{gr}} + \frac{1}{h_{cl}} \tag{3-58}$$

where $\Delta r_{gr}$ is the graphite thickness,

$$h_{cl} = \frac{k_{cl}}{D_{h-cl}} Nu_{cl} \tag{3-59}$$

and where

$D_{h\text{-}cl}$ = hydraulic diameter of the coolant channel, and
$Nu_{cl}$ = Nusselt number.

The fuel and graphite temperature during a transient are obtained by solving Eq. (3-55) and (3-57) with the coolant temperature treated as a forcing function. The coolant temperature is assumed to be given by

$$T_{cl} = \frac{T_{in} + T_{out}}{2} \tag{3-60}$$

where $T_{in}$ is the core inlet temperature and $T_{out}$ is the outlet temperature. These two quantities are obtained from an energy balance on the core solved in parallel with the conservation equations for the rest of the primary system. Implicitly differencing Eq. (3-55) gives

$$T_f^{n+1} - T_f^{n} = \frac{\Delta t\, Q_f^{n+1}}{(\rho C_p)_f} - \Delta t A_{11} T_f^{n+1} + \Delta t A_{11} T_{gr}^{n+1} \tag{3-61}$$

where

$$A_{11} = \frac{h_{f-gr} 2\pi r_f}{A_f (\rho C_p)_f} \ .$$

In the steady state the left-hand side is zero and the equation simplifies to

$$- A_{11} T_f + A_{11} T_{gr} + \frac{Q_f}{(\rho C_p)_f} = 0$$

Rearranging Eq. (3-61)

$$C_{11}\, T_f^{n+1} + C_{12}\, T_{gr}^{n+1} = D_1 \tag{3-62}$$

where

$$C_{11} = 1 + \Delta t A_{11}$$

$$C_{12} = - \Delta t A_{11}$$

$$D_1 = T_f^{n} + \Delta t \frac{Q_f^{n+1}}{(\rho C_p)_f} .$$

Implicitly differencing Eq. (3-57) gives

$$T_{gr}^{n+1} - T_{gr}^{n} = \Delta t\, A_{21} (T_f^{n+1} - T_{gr}^{n+1}) - \Delta t\, A_{23} (T_{gr}^{n+1} - T_{cl}^{n+1}) \tag{3-63}$$

where

$$A_{21} = \frac{h_{f-gr} 2\pi r_f}{A_{gr} (\rho C_p)_{gr}}$$

$$A_{23} = \frac{h_{gr\text{-}cl} 2\pi r_{gr}}{A_{gr} (\rho C_p)_{gr}} \quad .$$

In the steady state the left-hand side is zero and the equation simplifies to

$$A_{21}\, T_f - (A_{21} + A_{23})\, T_{gr} + A_{23}\, T_{cl} = 0$$

Rearranging Eq. (3-63)

$$C_{21}\, T_f^{n+1} + C_{22}\, T_{gr}^{n+1} = D_2 \tag{3-64}$$

where

$$C_{21} = -\Delta t A_{21}$$

$$C_{22} = \Delta t A_{21} + \Delta t A_{23} + 1$$

$$D_2 = \Delta t A_{23} T_{cl}^{n+1} + T_{gr}^{n}$$

These two equations for fuel and graphite temperature (either steady-state or transient case) are solved simultaneously with a coolant energy equation where $T_{cl}$ appears as an unknown and a fuel nuclear power equation where $Q_f$ appears as an unknown.

### 3.4.2 Reactivity Feedback

The net reactivity is expressed as a sum of individual reactivities. A reference state is defined and with it individual component temperatures. For convenience this state is taken as the full power steady-state condition. With respect to this state the reactivity introduced by a change in temperature of a component is given by

$$\rho = \frac{d\rho}{dL} L\, \beta\, \delta T \tag{3-65}$$

where is L is length, β is the coefficient of linear expansion, and δT is the temperature change. Of course, the individual component reactivities are dependent on the arrangement of components within the reactor vessel. We develop these for the GT-MHR upon which the VHTR is based. For this particular design 1) the reactor inlet coolant enters the core at the top and flows vertically down, 2) the control rod drive mechanisms are fixed to the top of the vessel and the rods enter at the top of the core, 3) the core rests on the bottom of the vessel, 4) the vessel wall is cooled by the coolant entering the reactor vessel, 5) the physical dimensions of the core are large compared to the neutron mean free path such that reactivity chage associated with a change in leakage due to core temperature expansion is insignificant, and 6) the reactivity feedback associated with coolant density is negligible.

#### 3.4.2.1 Control Rods

Temperature changes in the core introduce control rod reactivity in two ways. First, the vessel temperature is assumed equal to the reactor inlet temperature so the vessel length changes in response to reactor inlet temperature resulting a change in control rod position relative to the top of the core. Second, the temperature of the graphite moderator blocks are assumed equal to the coolant temperature so the core length changes in response to the coolant temperature resulting in a change in control rod position relative to the top of the core. The net change in reactivity is then given by

$$\delta\rho = (-(L\beta)_v\,\delta T_i + (L\beta)_m\,\delta T_m)\left(\frac{d\rho}{dL}\right)_{cr} \tag{3-66}$$

where

$T_i$ = reactor inlet coolant temperature and
$T_m$ = reactor midplane moderator temperature, and

where the last term is the change in reactivity per unit change in the position of the rods with respect to the top of the core. Insertion into the core is taken as the positive direction. The subscripts *v*, *m*, *cr* represent vessel, moderator, and control rod, respectively. The above expression is rewritten as

$$\delta\rho = \alpha_{cr-v}\,\delta T_i + \alpha_{cr-m}\,\delta T_m \tag{3-67}$$

where $\alpha_{cr-v} = -(L\beta)_v\left(\frac{d\rho}{dL}\right)_{cr}$ and $\alpha_{cr-m} = (L\beta)_m\left(\frac{d\rho}{dL}\right)_{cr}$ .

#### 3.4.2.2 Graphite Moderation

The neutron flux spectrum and neutron leakage change with graphite temperature creating a source of reactivity. Assuming the fuel temperature is maintained constant, the reactivity introduced relative to a reference graphite temperature is represented by

$$\delta\rho = \alpha_{gr-m}\,(T_{gr} - T_{gr,0}) \tag{3-68}$$

where $T_{gr}$ is the graphite midplane temperature. An estimate for the graphite moderator temperature coefficient of reactivity, $\alpha_{gr\text{-}m}$ is given in Table 5-20.

3.4.2.3 Coolant Density

A coolant density reactivity coefficient, $\alpha_{He}$ , is defined through

$$\rho_{void} - \rho_0 = \alpha_{He} (\theta_{void} - \theta_0) \tag{3-69}$$

where

$\rho$ = reactivity, and
$\theta$ = density.

The subscript *void* denotes the core with no coolant present and the subscript *0* denotes the full power reference condition. At the reference condition $\rho_0$ is taken as zero. The ideal gas law gives for the coolant at the core midplane,

$$\theta = \frac{P}{RT_{cl,K}} \tag{3-70}$$

where $T_{cl}$ is the reactor midplane coolant mixed-mean temperature in degrees Kelvin and P is the gas pressure. The reactivity change relative to the reference state for a change in temperature and pressure is then from Eqs. (3-69) and (3-70)

$$\rho = \frac{\alpha_{He}}{R}\left(\frac{P}{T_{cl}} - \left(\frac{P}{T_{cl}}\right)_0\right). \tag{3-71}$$

The coolant density reactivity coefficient can be solved for using Eqs. (3-69) and (3-71) is

$$\alpha_{He} = -R\left(\frac{T_{cl}}{P}\right)_0 \rho_{void} . \tag{3-72}$$

Typically, the coolant density reactivity coefficient is negligible in the thermal gas reactor and is set to zero in this work.

3.4.2.4 Fuel Doppler

The change in k-effective with the temperature of the fuel at the core midplane, $T_f$ , is given by

$$\frac{dk_{eff}}{dT_f} = \frac{K_D}{T_f} \tag{3-73}$$

where the left-hand side is the *Doppler coefficient* and $K_D$ is the *Doppler constant*. Integrating the above expression gives

$$\delta k_{eff} = K_D \ln\left(\frac{T_f}{T_{f,0}}\right) \tag{3-74}$$

where the subscript *0* denotes the full power steady-state condition. At this condition the net reactivity of the core is zero and $k_{eff}$ is unity. For a change from this state the new values of $\rho$ and $k_{eff}$ are related by

$$\rho = \frac{k_{eff} - 1}{k_{eff}} \approx \delta k_{eff} \tag{3-75}$$

where $\delta k_{eff}$ is the change in k-effective in going from full power steady state to the new state. Then from Eqs. (3-74) and (3-75), the reactivity in dollars from the change in fuel temperature is

$$\rho = \frac{K_D}{\beta_{eff}} \ln\left(\frac{T_f}{T_{f,0}}\right) \approx \alpha_D \, (T_f - T_{f,0}) \tag{3-76}$$

where

$$\alpha_D = \frac{K_D}{\beta_{eff} \, T_{f,0}}. \tag{3-77}$$

### 3.4.2.5 Net Reactivity

The net reactivity is the sum of the individual components given by Eqs. (3-67), (3-68), (3-71), and (3-76), plus any reactivity added through control rod motion not related to thermal expansion,

$$\rho = \alpha_{cr-v} \, (T_i - T_{i,0}) + (\alpha_{cr-gr} + \alpha_{gr-m}) \, (T_{gr} - T_{gr,0})$$

$$+ \frac{\alpha_{He}}{R}\left(\frac{P}{T_{cl}} - \left(\frac{P}{T_{cl}}\right)_0\right) + \alpha_D \, (T_f - T_{f,0}) + \rho_{rod}. \tag{3-78}$$

### 3.4.2.6 Net Reactivity in Quasi-Static Case

In the case where coolant, moderator, and fuel temperature are in equilibrium with the instantaneous power and flow, the above expression can be simplified. The total change in

reactivity due to temperature change is the sum of that associated with the control rods, the moderator, and the fuel and is given by

$$\delta\rho = \alpha_{cr-v}\,\delta T_i + \alpha_m\,\delta T_m + \alpha_{cr-m}\,\delta T_m + \alpha_f\,\delta T_f \tag{3-79}$$

where

$T_m$ = average moderator temperature.

Note that the moderator and fuel temperature changes are related to the reactor power-to-flow ratio and the reactor power through the expressions,

$$\delta T_m = \delta T_i + \frac{\Delta T_{c-100}}{2}\left(\frac{P}{W} - 1\right) + \Delta T_{m-100}(P-1), \tag{3-80}$$

$$\delta T_f = \delta T_i + \frac{\Delta T_{c-100}}{2}\left(\frac{P}{W} - 1\right) + (\Delta T_{m-100} + \Delta T_{f-100})\,(P-1)\,, \tag{3-81}$$

where

$P$ = fission plus decay power normalized to full power condition,
$W$ = flowrate normalized to full power condition,
$\Delta T_{c-100}$ = mixed mean reactor coolant temperature rise at full power condition,
$\Delta T_{m-100}$ = average moderator temperature rise at full power condition, and,
$\Delta T_{f-100}$ = average fuel temperature rise at full power condition.

If the feedback components in Eq. (3-79) are linear, then substituting the above expressions into Eq. (3-79) and collecting terms gives

$$\rho = (\alpha_{cr-v} + \alpha_m + \alpha_{cr-m} + \alpha_f)\,\delta T_i + (\alpha_m + \alpha_{cr-m} + \alpha_f)\frac{\Delta T_{c-100}}{2}\left(\frac{P}{W} - 1\right) + \alpha_f\,(\Delta T_{m-100} + \Delta T_{f-100})\,(P-1) \tag{3-82}$$

or

$$\delta\rho = A(P-1) + B\left(\frac{P}{W} - 1\right) + C\,\delta T_i \tag{3-83}$$

where

$$A = \alpha_f\,(\Delta T_{m-100} + \Delta T_{f-100}) \tag{3-84}$$

$$B = (\alpha_m + \alpha_{cr-m} + \alpha_f)\frac{\Delta T_{c-100}}{2}\,,$$

$$C = \alpha_{cr-v} + \alpha_m + \alpha_{cr-m} + \alpha_f \ .$$

3.4.2.7 Neutronic Time Constant

For the transients of interest the reactivity is always much less than $\beta$ so that the prompt jump approximation can be made. If also the number of precursor groups is taken as one, then the normalized fission power is given by

$$\left[\rho(t) - 1\right]\frac{dP}{dt} + \left[\lambda_f \rho(t) + \frac{d\rho}{dt}\right]P(t) = 0 \ . \tag{3-85}$$

where the reactivity has been normalized to $\beta$ and has units of dollars. The above equation is rearranged as

$$\frac{d}{dt}P = \frac{1}{\tau}P \tag{3-86}$$

and has solution

$$P = Ke^{t/\tau} \tag{3-87}$$

where

$$\tau = \frac{1-\rho}{\lambda\rho + \frac{d}{dt}\rho} \ . \tag{3-88}$$

The solution reveals the neutron population response has characteristic short and long term behavior. For a near step change in reactivity, in the short term as the reactivity is being added

$$\tau \approx \left(\frac{d}{dt}\rho\right)^{-1} \ . \tag{3-89}$$

Once the near step reactivity has been added, assuming $\rho << 1$, then

$$\tau \approx \frac{1}{\lambda\rho} \ . \tag{3-90}$$

which shows the approach to equilibrium proceeds initially with a time constant longer than that of the delayed neutron time constant followed by a continual lengthening.

An expression for the time constant of the core power when reactivity enters through reactivity feedbacks is obtained as follows. The reactivity is given by

$$\rho = A\left(P-1\right) + B\left(\frac{P}{W}-1\right) + C\delta T_{i} + \rho_{rod} \tag{3-91}$$

where the power, $P$, and flowrate, $W$, are normalized to some equilibrium condition. Here we have assumed that the core temperatures remain in equilibrium as power and flow change (in fact they will lag according to the thermal time constants of the structures that provide the reactivity feedback). From Eq. (3-86) and (3-90), if we let $P=1+\delta P$ , $W=1+\delta W$ , and drop other than first-order terms, then the power is given by

$$\frac{d}{dP}\delta P = \frac{1}{\tau}\delta P + \lambda\left[-B\delta W + C\delta T_{i} + \rho_{ext}\right], \quad \tau = \frac{-1}{\lambda\left(A+B\right)} . \tag{3-92}$$

# 4. INTERGATED PLANT POWER CONTROL SYSTEM

## 4.1 Reference Plant

The integrated system studied is described in [Davis 2006] as Case 6. In [Oh 2006] this design was selected as the reference case for the current project and in subsequent reports [Oh 2007] the design of the HTSE process was expanded upon to include specification of configuration of components and individual component sizes. In the present report a GAS-PASS/H code [Vilim 2004] model developed for the reference case and described in [Oh 2007] is used to calculate the full power condition and the partial power load schedule. That model is represented by the network diagrams shown in Figures 4-1 through 4-3.

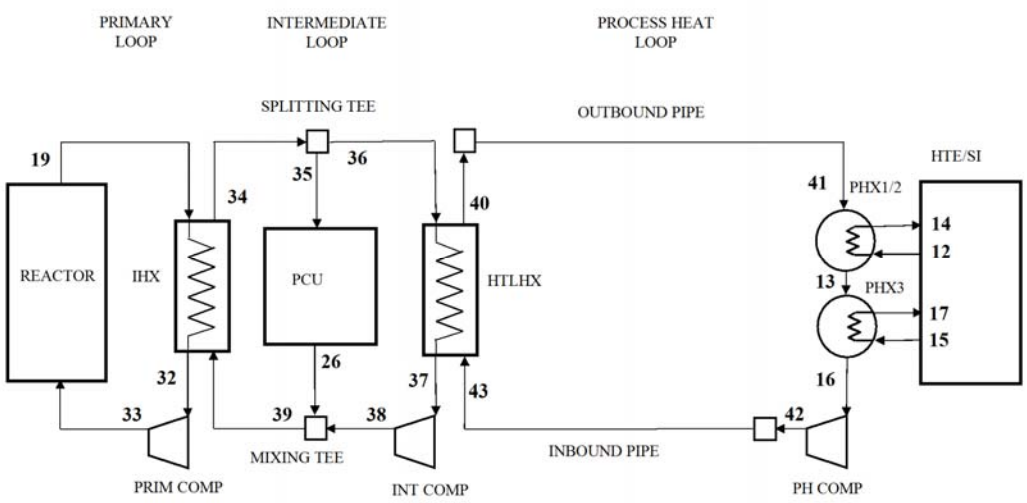


Figure 4-1 Overall Equipment Configuration for VHTR-HTSE Plant

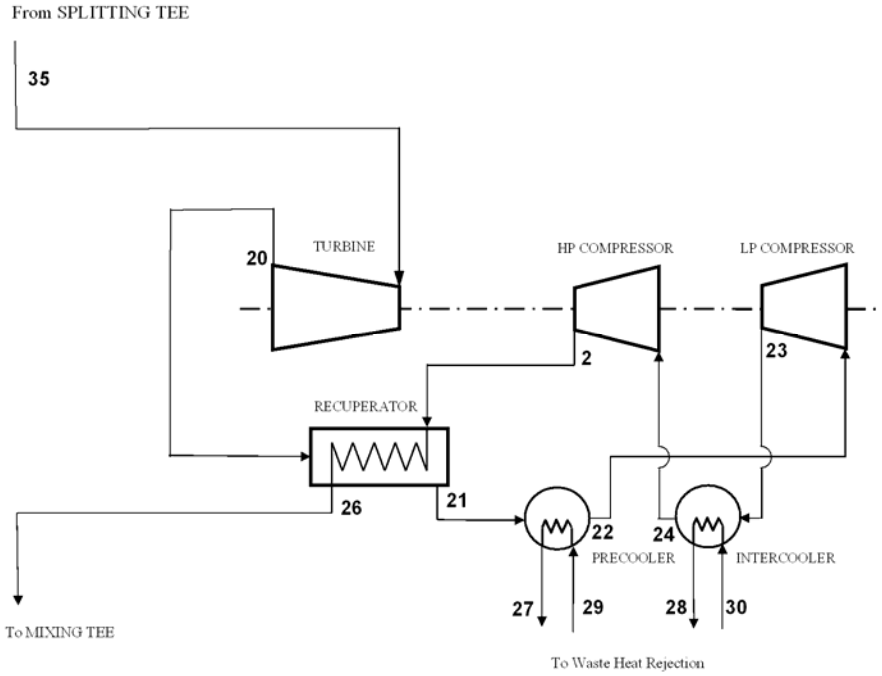


Figure 4-2 Power Conversion Unit Equipment Configuration

The first figure shows how the reactor, PCU, process heat loop, and HTSE plant are configured. The second figure shows the details of equipment layout for the PCU and the third figure the details of equipment layout for the HTSE plant.

The values of engineering parameters used in the simulation of the reference plant are given in Tables 4-1 through 4-3. Heat exchanger dimensions are given in Table 4-1. Compressor and turbine operating characteristics are given in Table 4-2. Electrolyser dimensions and operating characteristics are given in Table 4-3.

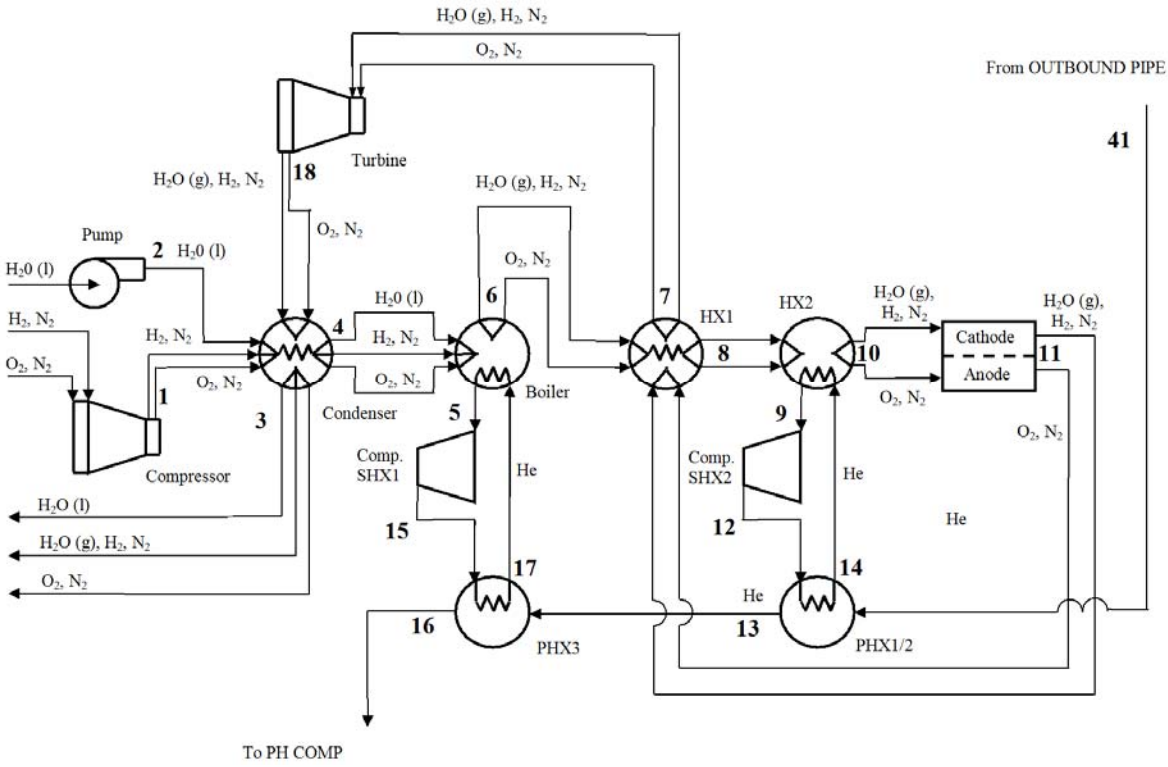


Figure 4-3 High Temperature Steam Electrolysis Equipment Configuration

## 4.2 Full-Power Design Point

A steady-state full power operating point was calculated with the GAS-PASS/H code model. The boundary conditions used are given in Table 4-4 and were selected based on consideration of the GT-MHR design as described in [Shenoy 1996], the operation of an HTSE plant as described in [Stoots 2005], and the integrated operation of the plants as described in [Davis 2006]. The values of process variables are given in Table 4-5 through 4-8. Conditions in the primary system are given in Table 4-5, conditions in the intermediate system in Table 4-6, conditions in the PCU in Table 4-7, and conditions in the HTSE plant in Table 4-8. The GAS-PASS/H code provides for a sweep gas but none was used in this model. The product stream into the electrolyzer was a boundary condition set to 0.95 and 0.05 mode fractions of $H_20$ and $H_2$, respectively. The value for the current boundary condition was selected to give a electrolyzer product output of 0.05 and 0.95 mode fractions of $H_20$ and $H_2$, respectively

Table 4-1. Design Data for Helium Printed Circuit Heat Exchangers

| | IHX | HTLHX | PCU Recuperator |
|---|---|---|---|
| Channel Diameter, *2r* (m) | 1.5e-03 | 1.5e-03 | 1.5e-03 |
| Channel Pitch, *P* (m) | 1.8e-03 | 2.25e-03 | 2.56e-03 |
| Plate Thickness, *t* (m) | 8.55e-04 | 1.17e-03 | 1.79e-03 |
| Channel Length, *l* (m) | 2.34 | 1.089 | 1.62 |
| Number of Channels, $N_{channels}$ (one side) | 7.33e06 | 4.36e05 | 4.264e06 |
| In Width Direction | 2639 | 673 | 2443 |
| In Height Direction | 2778 | 648 | 1745 |
| Hot Side Flow, *w* (kg/s) - Total | 289 | 32.1 | 260 |
| $w_{channel}$ - Per Channel | 3.94e-05 | 7.36e-05 | 5.10e-05 |
| Cold Side Flow, *w* (kg/s) - Total | 292 | 27.5 | 260 |
| $w_{channel}$ - Per Channel | 3.98e-05 | 5.31e-05 | 5.10e-05 |
| Width (m) | 4.75 | 1.52 | 5.23 |
| Height (m) | 4.75 | 1.52 | 5.23 |
| Volume ($m^3$) | 52.8 | 2.5 | 62.9 |

Table 4-2. Full Power Turbine and Compressor Operating Characteristics

| | | Pressure Ratio | Efficiency |
|---|---|---|---|
| Turbine - | HTSE | 3.2 | 0.93 |
| | PCU | 3.1 | 0.94 |
| Compressor - | Primary Loop | 1.014 | 0.89 |
| | Intermediate Loop | 1.014 | 0.89 |
| | Process Heat Loop | 1.17 | 0.89 |
| | PCU Low Pressure | 1.83 | 0.89 |
| | PCU High Pressure | 1.82 | 0.89 |

Table 4.3. Electrolyzer Dimensions and Operating Characteristics [Vilim 2006a]

| | $H_2O$ | $H_2$ | $O_2$ | | | |
|---|---|---|---|---|---|---|
| $A_w$ (kg/mol) | 18.0e-03 | 2.02e-3 | 32.0e-3 | | | |
| $C_\rho$ @ 950°C (J/kg-K) | 2.45e03 @50 atm | 15.1e3 @ 1 atm | 917 @ 1 atm | | | |
| A ($m^2$) | i (amps/$m^2$) | $(\rho V)_s$ [a] (kg) | $(C\rho)_s$ (J/kg-K) | $P/P_{STD}$ | T (C) | |
| 64e-4 | 1880 | 13.9e-3 | 400 | 50 | 816 | |
| F (coul/mol) | R (J/mol-K) | $\frac{(\partial \Delta G)^o}{\partial T}$ [b] (J/mol-K) | $ASR^o$ [c] (ohms-$cm^2$) | $C_1$ [c] (ohms-$m^2$) | $C_2$ [c] (K) | $\Delta G^o$ [b] (J/mol) |
| 96,485 | 8.31 | -55.5 @ 1 atm, 950°C | 0 | 8.39E-4 | 8,030 | 2.02e5 @ 1 atm, 950°C |

[a] [Hartivigsen 2006], [b] [Ohta 1979], [c] [Pradhan 2006]

Table 4-4. Boundary Conditions Used to Determine Full Power Operating Point

| Power (MW) | Reactor | Generator | | | | | |
|---|---|---|---|---|---|---|---|
| | 594 | 280 | | | | | |
| Temperature (°C) | HTSE Reactant Inlet | Precooler Cold Side Inlet | Intercooler Cold Side Inlet | | | | |
| | 21 | 21 | 21 | | | | |
| Flowrate (all species) (kg/s) | Electrolyzer Inlet | Compressor SHX1 | Compressor SHX2 | Precooler Cold Side Inlet | Intercooler Cold Side Inlet | Primary Compressor | Process Heat Loop Compressor |
| | 21.5 | 51.8 | 10.4 | 21 | 21 | 288 | 25.1 |
| Mode Fractions | Electroyzer Inlet – $H_2O$ | Electrolyzer Inlet – $H_2$ | | | | | |
| | 0.95 | 0.05 | | | | | |
| Current (amps) | Electrolyzer | | | | | | |
| | 217 | | | | | | |

Table 4-5. Primary System Full Power Conditions

| | Reactor | IHX Hot Side | Primary System Compressor |
|---|---|---|---|
| Power (MW) | 594 | 601 | 7 |
| Outlet Temperature (°C) | 887 | 485 | 490 |
| Outlet Pressure (MPa) | 7.09 | 7.04 | 7.13 |
| Mass Flowrate (kg/s) | 288 | 288 | 288 |

Table 4-6. Intermediate System Full Power Conditions

| | IHX Cold Side | HTLHX Hot Side | Mixing T | Intermediate Compressor |
|---|---|---|---|---|
| Power (MW) | 601 | 436 | 0 | 0.9 |
| Outlet Temperature (°C) | 485 | 611 | 478 | 617 |
| Outlet Pressure (MPa) | 7.04 | 7.27 | 7.37 | 7.37 |
| Mass Flowrate (kg/s) | 288 | 32.4 | 291 | 32.4 |

Table 4-7. Power Conversion Unit Full Power Conditions

| | Turbine | Recuperator Hot Side | Recuperator Cold Side | HP Compressor | LP Compressor | Precooler Hot Side | Inter-cooler Hot Side |
|---|---|---|---|---|---|---|---|
| Power (MW) | 534 | 462 | 462 | 126 | 127 | 151 | 127 |
| Outlet Temperature (°C) | 479 | 141 | 461 | 123 | 124 | 30 | 30 |
| Outlet Pressure (MPa) | 2.36 | 2.31 | 7.37 | 7.43 | 4.13 | 2.26 | 4.08 |
| Mass Flow Rate (kg/s) | 263 | 263 | 263 | 263 | 263 | 263 | 263 |

Table 4-8. High Temperature Steam Electrolysis Plant Full Power Conditions

| | | Condenser | Boiler | HX1 | HX2 | Turbine | Cell | PHX1/2 | PHX3 |
|---|---|---|---|---|---|---|---|---|---|
| Power (MW) | Hot Side | 18.8 | 43.2 | 24.9 | 5.32 | 11.5 | 288 | 5.3 | 43.2 |
| | Cold Side | 18.8 | 43.2 | 24.9 | 5.32 | | | 5.3 | 43.2 |
| Outlet Temperature (°C) | Hot Side | 43 | 328 | 545 | 725 | 340 | 968 | 800 | 469 |
| | Cold Side | 184 | 247 | 712 | 817 | | | 842 | 488 |
| Outlet Pressure (MPa) | Hot Side | 1.53 | 5.0 | 5.0 | 5.0 | 1.56 | 5.0 | 1.76 | 1.71 |
| | Cold Side | 5.00 | 5.0 | 5.0 | 5.0 | | | 5.0 | 5.0 |
| Mass Flowrate - All Species (kg/s) | Hot Side | 21.5 | 51.8 | 21.5 | 10.4 | 21.5 | 21.5 | 25.1 | 25.1 |
| | Cold Side | 21.5 | 21.5 | 21.5 | 21.5 | | | 10.4 | 51.8 |

## 4.3 Power Control Scheme

The integrated system must be capable of operating to meet production demands that originate beyond the plant fence, most likely from the operator of a hydrogen pipeline or storage facility. This necessarily implies the plant must be able to startup and shutdown and meet partial production demands. In this section control schemes for operating the plant at partial production levels are described. It considers the quasi-static case where production levels are changed in a slow enough manner that dynamics are not excited. More rapid changes in load are addressed in the next section. Control schemes are developed for meeting hydrogen production rates that lie in the range 30 to 100 percent of full power production. It is possible that yet to be performed research on energy systems and their mix in the U.S. may conclude that there is no requirement for partial load operation. Perhaps operation between only 80 and 100 percent full power, as is typical for a chemical plant, will be all that is needed. Modeling and simulating startup and shutdown is more complex as described in Section 2.4. This task will be performed later in this project.

A main objective in developing a control strategy for partial load operation is to maintain temperatures, particularly hot end temperatures (~ 900 C), constant with power over the 30-100 percent power range. Another consideration is that peak efficiency occurs at full power since the plant is to operate there for the largest fraction of life. While partial load efficiency is important, maintaining constant temperatures over load at the hot end is probably more important since material capabilities at 900 C are a limiting factor in plant lifetime. Development of a control strategy is therefore focused on maintaining constant hot end temperatures.

The first control strategy examined makes use of the principle that the temperature change from inlet to outlet in a heat exchanger remains constant when the mass flowrate and power are varied in the same proportion. This is true for ideal-like gases such as helium, hydrogen, oxygen, and nitrogen and for the liquid and gas phases of water. It is not true, however, for water when there is a phase change. In the HTSE plant and its process heat loop there are a total of five compressor and pumps with which to manage mass flowrate in response to power in heat exchangers (to the first order heat exchanger power varies linearly with hydrogen production rate). In the PCU and primary system there is only one compressor to manage mass flowrate while there are several different circuits. To achieve the desired control of mass flowrate helium inventory control is used. Essentially because density is proportional to pressure for fixed temperature, by varying pressure and maintaining constant speed turbomachinery, gas velocity remains constant and mass flowrate (proportional to the product of density and velocity) is linear with pressure. Thus, pressure is manipulated through coolant mass inventory so that it is proportional to heat exchanger power so that in turn mass flowrate is proportional to heat exchanger power. The result for this control scheme is described below.

A load schedule was formulated to give the value of all process variables in terms of fraction of full power hydrogen production rate. The control scheme that realizes this prescribes all controlling process variables (i.e. forcing functions) as a function of fraction of full power hydrogen production rate which is taken as the independent variable (or equivalently, electrolyzer electrical current where it has been assumed all current goes to decompose water). The following controlling process variables were selected: reactor power, eight mass flowrates, plus the electrolyzer current, for a total of ten forcing functions. The need for ten forcing functions follows from the number of equations in the model and the dictate that there be a unique solution. As a cross check, the number of forcing functions needed was independently derived from consideration of the physics alone. Other sets of ten could be used but this set was appealing based on the discussion above. Each of these ten forcing functions was linearly ramped from its full power value at one end to a value of 30 percent of this at the other end. Hence, the load schedule covers the range of operation from 30 to 100 percent of the full power hydrogen production rate.

The load schedule is assessed primarily on the degree to which temperatures on the hot side of the combined plant are maintained constant. Also of interest are the pressures on the helium side for assessment of creep under pressure load. The pressures in the HTSE plant were maintained at 5 MPa over the load schedule from downstream of where the reactant water in fed in up to the point where the products enter the pressure-work recovery turbine.

The temperatures in the hot side of the plant are shown in Figures 4-4 and 4-5. The first figure shows the temperatures in the HTSE plant and the second figure shows temperatures in the VHTR plant. The temperatures in the latter vary by no more than 30 C over the load range. However, in the HTSE plant, the electrolyzer outlet varies by more than 400 C over the load range. The inlet to the electrolyzer is essentially constant temperature. Other temperatures in the HTSE plant vary by 100 to 200 C. These

temperature changes with load, especially at the electrolyzer outlet are probably not acceptable since they will limit the rate at which the plant could change power. Cold side temperatures in the combined plant are shown in Figure 4-6. The largest temperature change is about 150 C in the process heat loop inbound pipe. Helium loop pressures are shown in Figure 4-7. Pressure is to a first order proportional to hydrogen production rate, a consequence of inventory control. The production and consumption of power by major system components is shown in Figure 4-8. Essentially all the thermal power produced by the VHTR is consumed by thermal loads in the HTSE plant and in generating electricity to power electrical loads which include the electrolyzer and pumps and compressors. But as described in [Vilim 2007], there is a potential for supplanting some of the thermal load with waste heat so that the combined plant could be a net exporter of electricity to the grid.

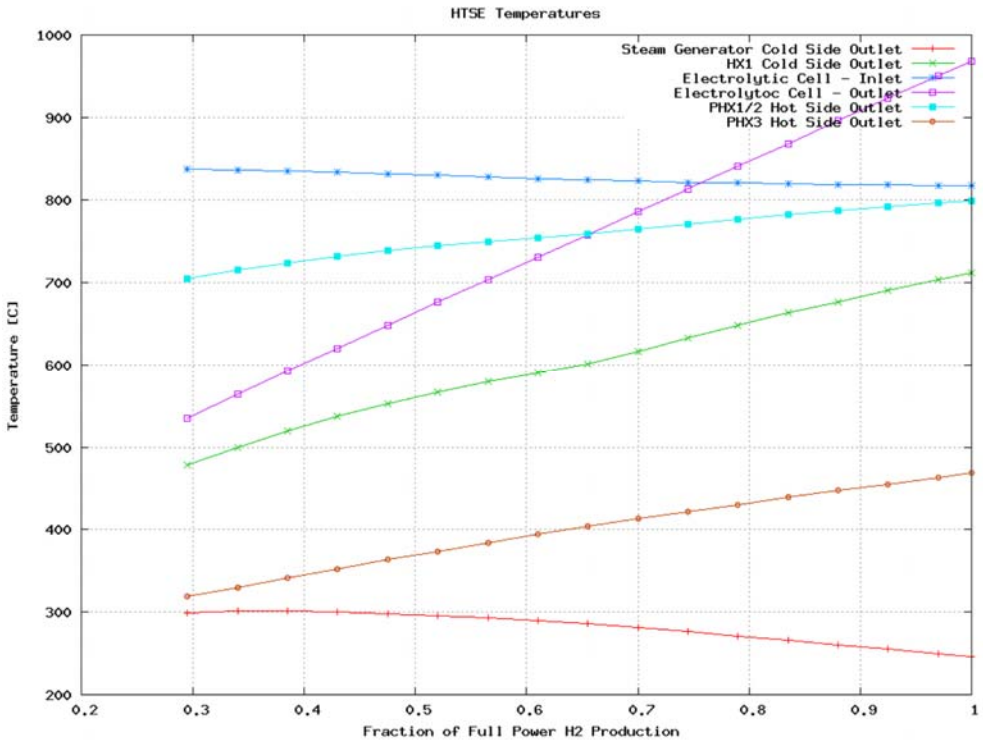


Figure 4-4 Temperatures in High Temperature Steam Electrolysis Plant

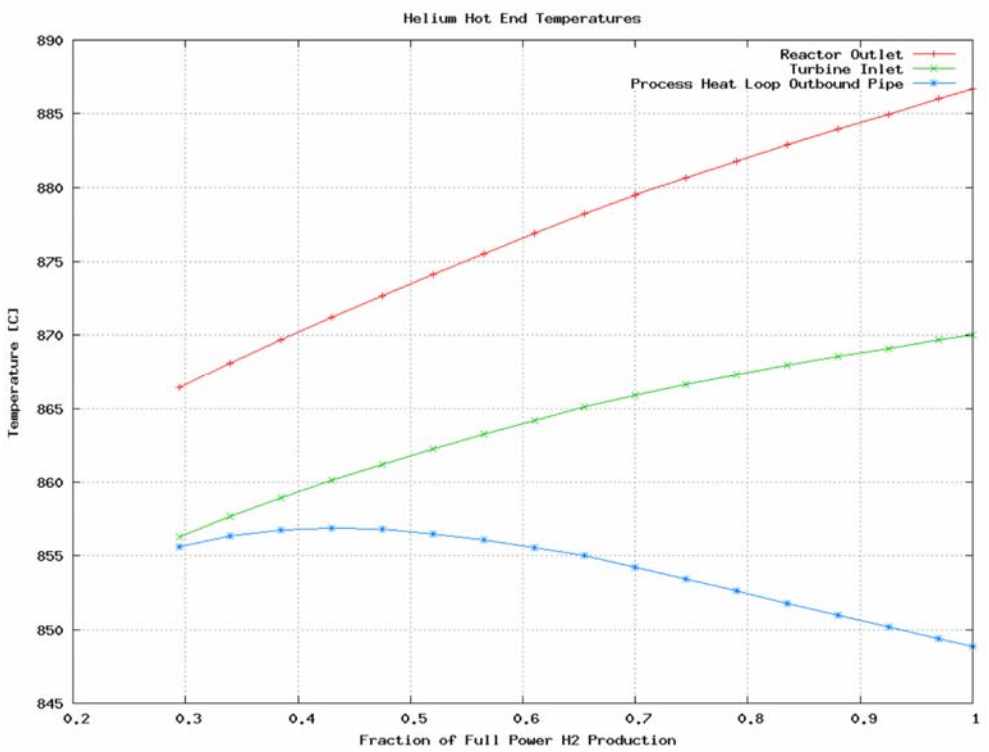


Figure 4-5 Temperatures in Hot End of VHTR Plant

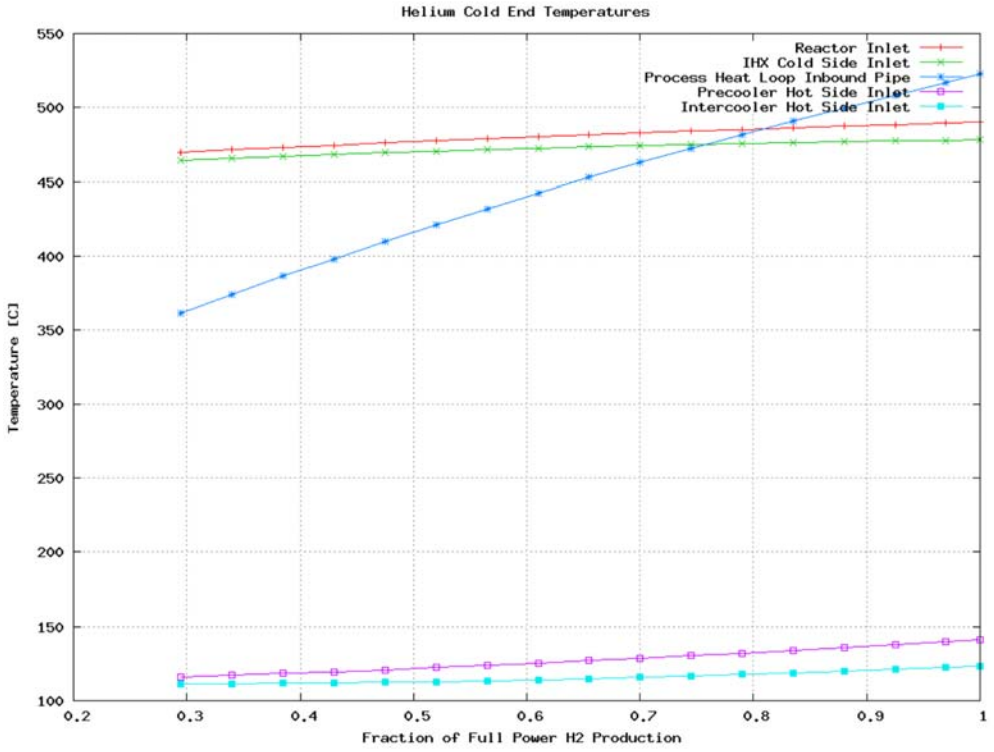


Figure 4-6 Temperatures in Cold End of VHTR Plant

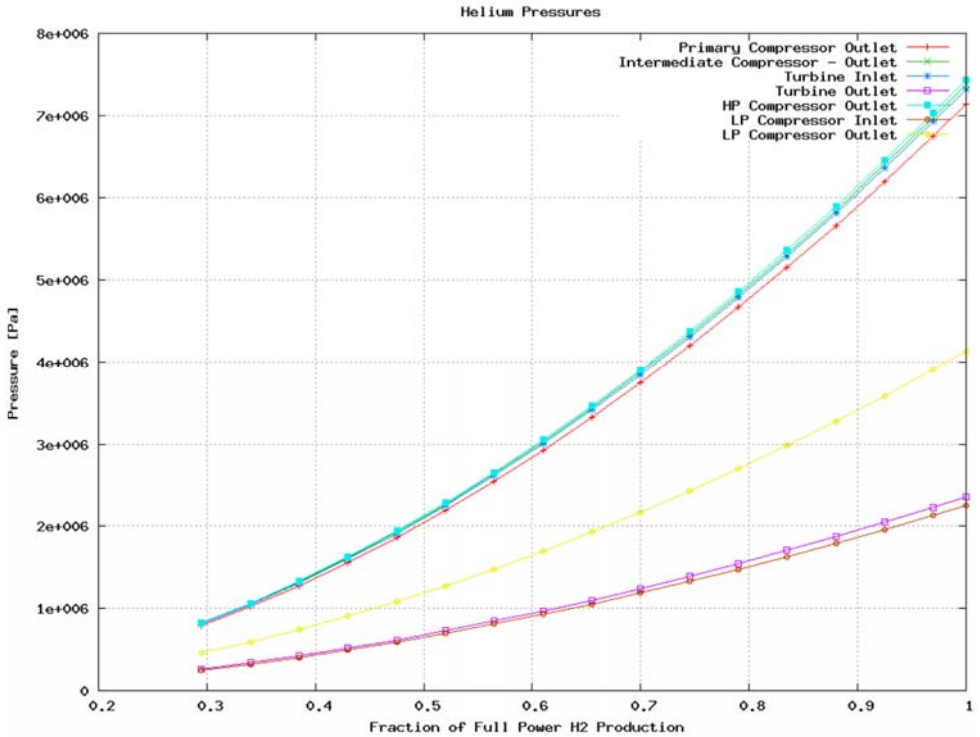


Figure 4-7 Pressures in Helium Loops

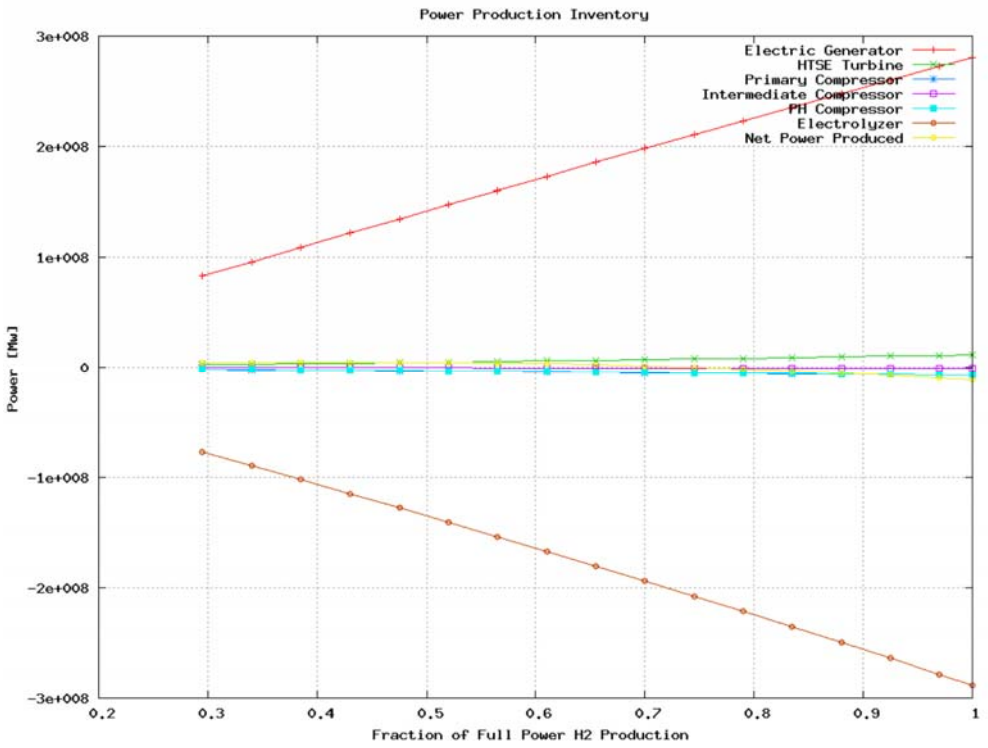


Figure 4-8 Power Production and Consumption in Major System Components

Because the electrolyzer sensible heat is recuperated externally at the exit of the recuperator, there is a significant temperature rise in the electrolyzer during full power operation. If the resulting spatial temperature gradient is unacceptable, then either internal recuperation or operating the cell at a current density where there is no sensible heat generated along the length between inlet and outlet can be used to reduce the size of the gradient. The latter option has the disadvantage that the required current density will be lower resulting in an increase in cell area per unit hydrogen production rate and poorer economics. Internal recuperation would seem to be the preferred solution since it involves only passing a counter current gas flow over the individual cells lined up from inlet to outlet.

With the control strategy just described the outlet temperature of the electrolyzer varies significantly (~ 400 C) over the 30-100 percent hydrogen production range. The sensible or joule heat depends near linearly on the hydrogen production rate for constant current density. Thus, by maintaining constant current density as hydrogen production rate varies the cell temperature rise from inlet to outlet will be constant. Constant current density can be achieved by maintaining constant active cell area per unit hydrogen production (i.e operate fewer cells as production rate decreases). This scheme was explored with GAS-PASS/H. The results are shown in Figure 4-9 through 4-11. Clearly, this is effective as seen in Figure 4-9 where the ranges of electrolyzer inlet and outlet temperature have been significantly reduced.

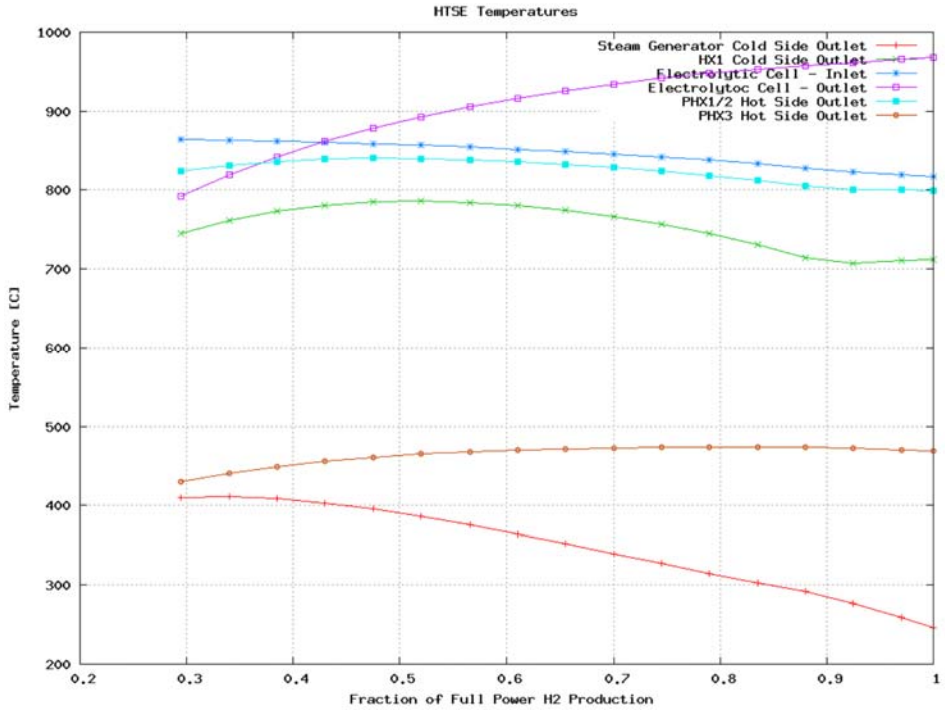


Figure 4-9 Temperatures in High Temperature Steam Electrolysis Plant for Reduced Cell Area

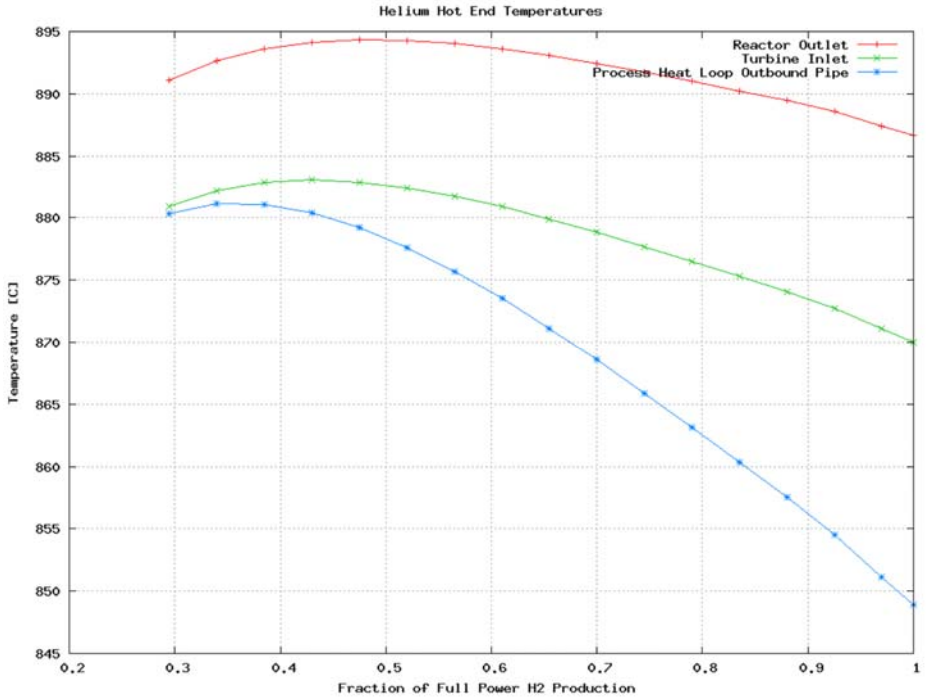


Figure 4-10 Temperatures in Hot End of VHTR Plant for Reduced Cell Area

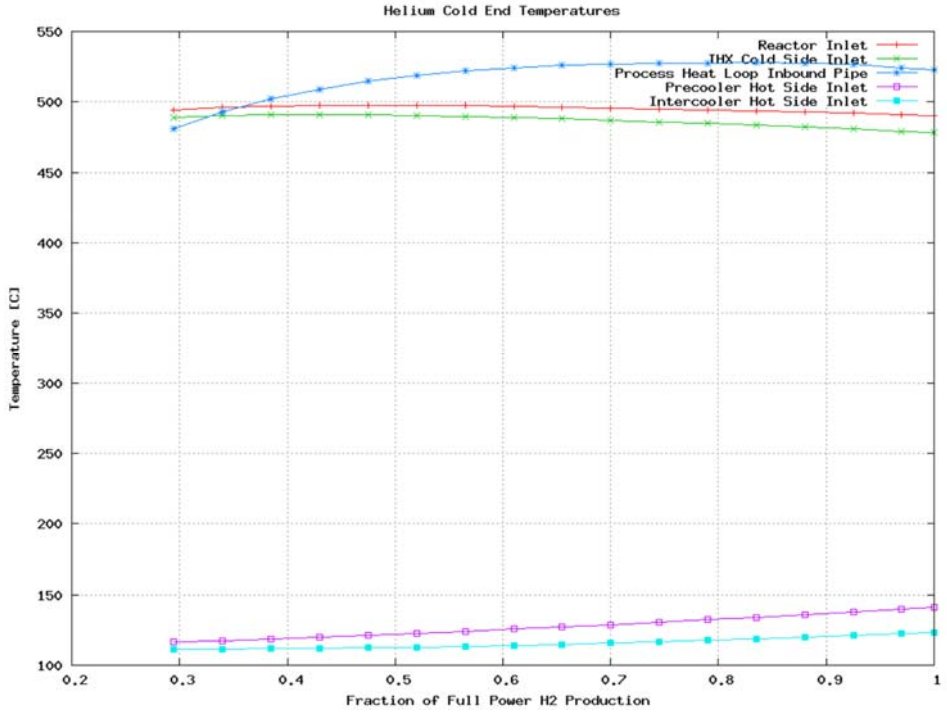


Figure 4-11 Temperatures in Cold End of VHTR Plant for Reduced Cell Area

The electrolyzer outlet temperature range is now 180 C, down from over 400 C. These results were obtained for a linear ramp in cell area starting with the previous value at full

power value down to a fraction 0.4 at 30 percent hydrogen production rate. There is also a reduction in the temperature variation in the process heat inbound pipe as seen by comparing Figure 4-6 with Figure 4-11. In general then, managing active cell area during load change can lead to a reduction in temperature swings seen in components.

In Section 2.3 the mathematical basis for obtaining a desired load schedule is given. From this development it is clear that a combination of flowrate (compressor and pump) and current density control should permit the results in Figures 4-9 through 4-11 to be refined so that hot end temperature changes with load are further reduced. This is left for future work.

# 5. PLANT TRANSIENT BEHAVIOR

## 5.1 Time Constants and Energy Capacitances

### 5.1.1 Electrolyzer

The cell time constant of Section 3.1 is evaluated for representative VHTR/HTSE cell conditions. For simplicity it was assumed the reactant stream is pure water vapor and that it is completely decomposed in the cell. The data input to the calculation are shown in Tables 5-1 through 5-3. It is assumed the reactant stream is pure water vapor and that it is completely decomposed by the cell as shown in Table 5-1. Representative operating conditions are given in Table 5-2. The values for cell mass and specific heat include only the electrodes and the electrolyte and not the separators, edge rails, or flow forms according to the rationale given earlier. The cell mass is from [Hartvigsen 2006]. The ASR data is from [Pradhan 2006]. The expression for the cell time constant (Eq. (3-14)) yielded a value of 206 s for this data.

The cell energy capacitance of Section 3.1 is also evaluated for representative VHTR/HTSE cell conditions. The mass of a cell of electrode area 64 $cm^2$ as obtained from [Hartvigen 2006] was multiplied by the estimated specific heat of the cell material and the number of such cells to obtain the energy capacitance. The number of cells was obtained by taking the total electrode area in Table 5-4 and dividing by 64 $cm^2$. The calculation is shown in Table 5-4 and yields a value of 270 J/K. It should be noted, however, that design optimization has not yet been performed and so electrode area is subject to some uncertainty. More aggressive operation of the cell could reduce total electrode area by up to a factor of ten compared to the value given in Table 5-4. The estimated thermal capacitance would decrease by this same factor. The time constant and energy capacitance values have been entered in Table 5-22.

The validity of assumptions made in the derivation of the one-dimensional model of Section 3.1 has been examined. The model ignores the two-dimensional nature of the temperature distributions in the electrodes, electrolyte, and gas streams that arise as a consequence of the planar rectangular geometry of the cell and the 90 degree difference in angle of incidence between the two gas streams. In addition the heat capacity of the steel separators and edge rails is neglected since their temperature state is thought to be not tightly thermally coupled to the electrodes and electrolyte.

An experiment [Pradhan 2006] provided an opportunity to validate the expression for the time constant given by Eq. (3-14). In the experiment the identical Cerametec cell that is being used for water splitting SOEC studies at Idaho National Laboratory (INL) was run in fuel cell mode. The conditions are the same as in Table 5-1 through 5-3 with the exception that the pressure was atmospheric and that hydrogen and oxygen were fed into the cell rather than removed from the cell. The cell was operated at atmospheric pressure and hydrogen and oxygen were fed into rather than removed from the cell. The mole fractions of hydrogen, oxygen, and water estimated from [Pradhan 2006] were 0.46, 0.2, and 0.85. The water-splitting model in Section 3.1 was modified to describe a fuel cell

by a change of sign on the Nernst potential and the Gibbs standard free energy of formation (to account for interchange of products and reactants). With these adjustments and for the conditions in [Pradhan 2006] Eq. (3-14) yields a cell time constant of 279 s.

A value for the time constant of the cell was derived from data in [Pradhan 2006] by empirical curve fitting. In the experiment the fuel cell was at a steady state prior to a step change in the cell current. The measured cell outlet temperature during the subsequent transient appears in Figure 5-1. The description in [Pradhan 2006] indicates there was an initial power supply problem and, hence, the appearance of a saw tooth on the ramp up in temperature. We have attempted to adjust for this by backward extrapolating in time after the occurrence of the sawtooth. Figure 5-1 shows the back calculation of a value for the time constant from the experiment data. The value from Eq. (3-14) (i.e. 279 s as given above) differs by 19 percent from the value of 235 s obtained from Figure 5-1 by curve fitting. This suggests that the assumptions underlying the derivation in Section 3.1 are reasonable from the standpoint of estimating an approximate measure of cell outlet temperature time response.

Table 5-1 Species Data for Electrolytic Cell Time Constant Estimate

| | $H_2O$ | $H_2$ | $O_2$ |
|---|---|---|---|
| $A_w$ (kg/mol) | 18.0e-3 | 2.02e-3 | 32.0e-3 |
| $C_\rho$ @ 950°C (J/kg-K) | 2.45e+3 @50 atm | 15.1e3 @1 atm | 917 @1 atm |
| F | 1.0 | 0.67 | 0.33 |

Table 5-2 Operating Data for Electrolytic Cell Time Constant Estimate

| A ($m^2$) | i (amps/$m^2$) | $(\rho V)_s$[c] (kg) | $(C_\rho)_s$ (J/kg-K) | $P/P_{STD}$ | T (C) |
|---|---|---|---|---|---|
| 64e-4 | 1880 | 13.9e-3 | 400 | 50 | 816 |

[a] [Hartivigsen 2006]

Table 5-3 Other Data for Electrolytic Cell Time Constant Estimate

| F (coul/mol) | R (J/mol-K) | $\frac{(\partial \Delta G)^o}{\partial T}$ [a] (J/mol-K) | $ASR_o$ [b] (ohms-$cm^2$) | $C_1$ [b] (ohms-$m^2$) | $C_2$ [b] (K) | $\Delta G^o$ [a] (J/mol) |
|---|---|---|---|---|---|---|
| 96,485 | 8.31 | -55.5 @1 atm, 950°C | 0 | 8.39e-4 | 8,030 | 2.02e5 @1 atm, 950°C |

[a][Ohta 1979] [b][Pradhan 2006] [c][Hartvigsen 2006] (electrodes and electrolyte)

Table 5-4 Electrolytic Cell Time Constant and Energy Capacitance

| T (s) | Cell area = 225 $cm^2$ | | Cell area =64 $cm^2$ | | |
|---|---|---|---|---|---|
| | No. of cells[b] | Stack Electrode Area ($m^2$) | No. of Cells | $(\rho V)_s (C_\rho)_s$ per Cell (J/K) | Total[a] $(\rho V)_s (C_\rho)_s$ (J/K) |
| 206 | 14e06 | 0.0225*14e06= 3.15e5 | 3.15e5/0.0064= 49.2e06 | 13.9e-03*400= 5.56 | 5.56*49.2e06= 270e06 |

[a] Electrodes and electrolyte only

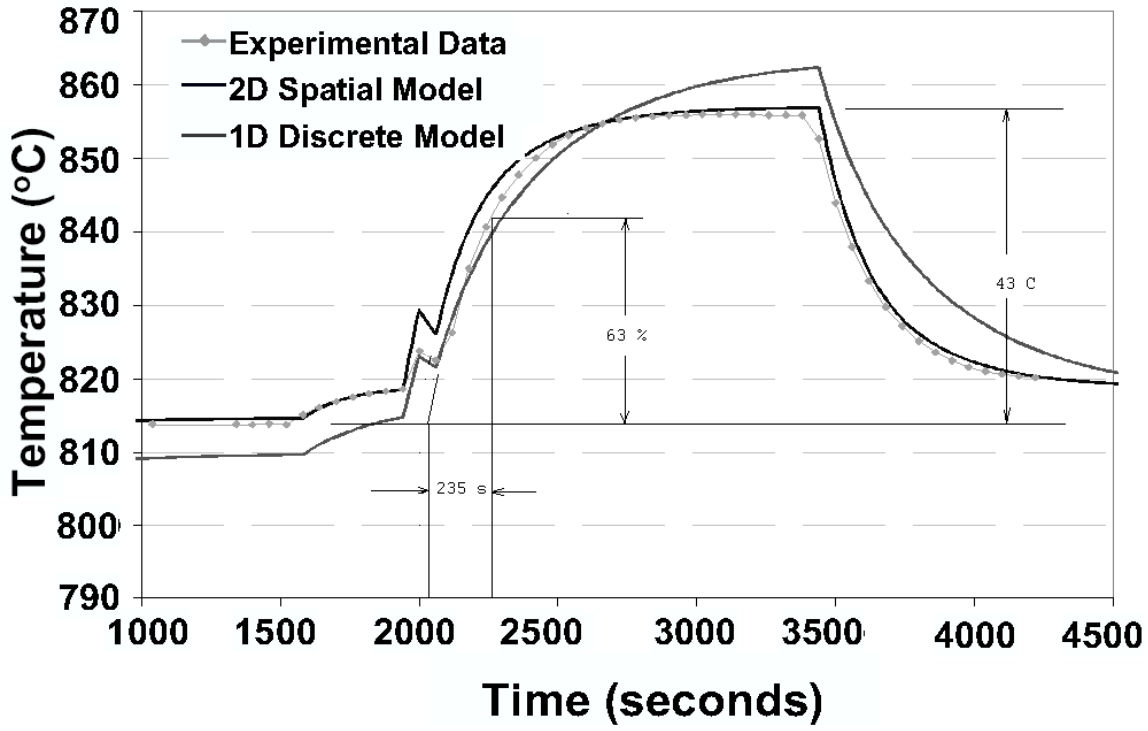


Figure 5-1 Time Constant for an Electrolytic Cell Operating in the Fuel Cell Mode

### 5.1.2 PCHE Heat Exchangers

As described previously there are incentives to choose printed circuit type heat exchangers for heat transfer circuits that use a gas coolant. In the reference configuration for the combined plant shown in Figure 4-1 the recuperator in the PCU and heat exchangers IHX and HTLHX are assumed to be PCHEs. Time constants and energy capacitances are calculated for these units from the models developed in Section 3.2.

Design data for these heat exchangers are taken from [Oh 2006a] and are reproduced in Table 5-5. Thermo-physical properties used in the calculation are given in Table 5-6. Values for heat transfer parameters associated with the models of Section 3.2 are given in Table 5-7. The three time constants associated with the hot side of the PCHE are shown in Table 5-8. Note that there are corresponding time constants not shown for the cold side. They were not calculated as their values will be similar to those for the hot side.

Inspection of Table 5-8 shows that the heat exchanger metal has an energy capacitance at least five times greater than the next highest source of capacitance. The time constants associated with the other capacitances are at least a factor of ten faster than for the metal. Thus, the heat exchanger response is dominated by the metal behavior. Table 5-9 shows the calculation of the metal capacitance. The cold side metal is accounted for by doubling the capacitance of the hot side metal. The time constants shown are those for the metal taken from Table 5-8. This data is reproduced in Table 5-22.

Table 5-5 Design Data for Helium Printed Circuit Heat Exchangers [Oh 2006a]

| | IHX | HTLHX | PCU Recuperator |
|---|---|---|---|
| Channel Diameter, $2r$ (m) | 1.5e-03 | 1.5e-03 | 1.5e-03 |
| Channel Pitch, $P$ (m) | 1.8e-03 | 2.25e-03 | 2.56e-03 |
| Plate Thickness, $t$ (m) | 8.55e-04 | 1.17e-03 | 1.79e-03 |
| Channel Length, $l$ (m) | 2.34 | 1.089 | 1.62 |
| Number of Channels, $N_{channels}$ (one side) | 7.33e06 | 4.36e05 | 4.264e06 |
| In Width Direction | 2639 | 673 | 2443 |
| In Height Direction | 2778 | 648 | 1745 |
| Hot Side Flow, $w$ (kg/s) - Total | 289 | 32.1 | 260 |
| $w_{channel}$ - Per Channel | 3.94e-05 | 7.36e-05 | 6.10e-05 |
| Cold Side Flow, $w$ (kg/s) - Total | 292 | 27.5 | 260 |
| $w_{channel}$ - Per Channel | 3.98e-05 | 6.31e-05 | 6.10e-05 |
| Width (m) | 4.75 | 1.52 | 6.23 |
| Height (m) | 4.75 | 1.52 | 6.23 |
| Volume ($m^3$) | 52.8 | 2.5 | 62.9 |

Table 5-6 Thermo-Physical Properties for Helium Printed Circuit Heat Exchangers

| | IHX | HTLHX | PCU Recuperator |
|---|---|---|---|
| $(C_p)_m$ (J/kg-K) | 500 | 500 | 500 |
| $(C_v)_h = (C_p)_h - R$ (J/kg-K) | 3114 | 3114 | 3114 |
| $(C_p)_h$ (J/kg-K) | 5200 | 5200 | 5200 |
| $\rho_h$ (kg/m$^3$) | 3.59 | 3.47 | 2.18 |
| $\rho_m$ (kg/m$^3$) | 8000 | 8000 | 8000 |
| $k_m$ (J/m-s-K) | 22 | 23 | 16.4 |

Table 5-7 Hot-Side Heat Transfer Parameters for Helium Printed Circuit Heat Exchangers

| | IHX | HTLHX | PCU Recuperator |
|---|---|---|---|
| θ (rads), Eq. (13) | 0.285 | 0.285 | 0.285 |
| $C_h$ (m), Eq. (14) | 0.00193 | 0.00193 | 0.00193 |
| $A_h$ (m$^2$), Eq. (14) | 5.71e-07 | 5.71e-07 | 5.71e-07 |
| $h_{h-m}$ (J/m-s-K) (Ref. C. Oh) | 1660 | 1715 | 2089 |
| $\bar{h}_{h-m}$ (J/m-s-K), Eq. (4) | 2.82 | 3.1 | 3.61 |
| $A_m$ (m$^2$) | 1.98e-07 | 7.45e-07 | 1.72e-06 |

Table 5-8 Time Constants for Helium Printed Circuit Heat Exchangers

| | IHX | HTLHX | PCU Recuperator |
|---|---|---|---|
| $(\rho A l C_v)_h$ (joules/$^o$C) | 0.0150 | 0.00672 | 0.00628 |
| $(C_p w)_h$ | 2.05e-01 | 3.83e-01 | 3.17e-01 |
| $(\rho A C_v)_h$ | 0.00638 | 0.00617 | 0.00388 |
| $(\rho A C_p)_m$ | 7.94e-01 | 2.98 | 6.88 |
| $\tau_{i-h} = \frac{(\rho A l C_v)_h}{(C_p w)_h}$ (s) | 0.07 | 0.02 | 0.02 |
| $\tau_{h-m} = \frac{(\rho A C_v)_h}{\bar{h}_{h-m}}$ (s) | 0.002 | 0.002 | 0.001 |
| $\tau_{m-h} = \frac{(\rho A C_p)_m}{\bar{h}_{h-m}}$ (s) | 0.28 | 0.96 | 1.9 |

Table 5-9 PCHE Time Constant and Energy Capacitance

| | IHX | HTLHX | PCU Recuperator |
|---|---|---|---|
| Metal Energy Capacitance $(\rho A C_p)_m$ per channel (J/C-m) | 7.94e-01 | 2.98 | 6.88 |
| Channel Length, $l$ (m) | 2.34 | 1.089 | 1.62 |
| Number of Channels, $N_{channels}$ (one side) | 7.33e06 | 4.36e05 | 4.264e06 |
| Total Capacitance, $2\ (\rho A C_p)_m\ l\ N_{channels}$ (MJ/C) | 27 | 2.8 | 95 |
| Dominant Time Constant | 0.28 | 0.96 | 1.9 |

### 5.1.3 Boiler

The expression for the boiler time constant given by Eq. (3-53) is dependent on the internal geometry and dimensions of the heat exchanger. At this time the boiler design is known only to the level of thermal power and UA. Rather than perform a detailed design effort to obtain this additional data, engineering scaling principles are applied to a unit for which a complete design is available. The unit is the 300 MWt Oconee once-through steam generator for which a dynamic model was developed in [Vilim 2001]. The temperatures and pressure conditions used in this model are similar to those in the HTE plant while the heat transfer rate is based on heat transfer correlations. So it is expected the numbers obtained should be representative for the purposes of scoping calculations.

The Oconee unit and related model [Vilim 2001] additionally have subcooled and superheat regions. It is advantageous then not limit to limit treatment of the time constant to just the boiler, but to set up a similar correspondence between HTSE superheater and condenser components with once-through steam generator superheated and subcooled regions, respectively. Note that since the condensation heat rate in the HTSE condenser is a small fraction of the component heat load, it will be ignored. The condenser can then be treated as a heat exchanger with subcooled water on one side and vapor on the other and data obtained from the subcooled region of the once-through steam generator.

In obtaining the heat exchanger data from the correspondences defined above, the assumption is made that the heat transfer coefficient in each of the superheater (HX1), boiler, and condenser in Figure 4-3 has the same value as in the corresponding regions of the Oconee model. This is a reasonable assumption since the underlying heat transfer mechanisms are the same between corresponding regions. In this case, individually for each region

$$\left(\frac{Q}{A\,\Delta T}\right)_{OT} = \left(\frac{Q}{A\,\Delta T}\right)_{HTSE} \tag{5-1}$$

where $Q$ is the thermal power, $A$ is the heat transfer coefficient, and $\Delta T$ is the log mean temperature difference and subscript $OT$ represents once-through. The heat transfer areas are then related through

$$\frac{A_{HTSE}}{A_{OT}} = \left(\frac{Q}{\Delta T}\right)_{HTSE} \left(\frac{\Delta T}{Q}\right)_{OT} . \tag{5-2}$$

This scaling law is used to obtain HTSE design data from the once-through design.

The area scaling factor on the left-hand side of the above equation is calculated for each of the HTSE condenser, boiler, and superheater. These components appear in Figure 4-3 and the data used are from the HTSE plant data in Table 4-8 and the once-through unit in [Vilim 2001]. Note that the HTSE plant contains superheaters HX1 and HX2 having thermal power 26 and 5 MWt, respectively. For the purposes of computing time constants and energy capacitances, HX2 is ignored because its effect on time behavior is second order. The input data and the calculated values of the area scaling factor are shown in Table 5-10. Note the expression for the log mean temperature difference, $\Delta T$, differs between the single phase and two-phase cases.

In applying the area scaling factor to compute heat exchanger dimensions, it is assumed the adjusted area in going from once-through to HTSE plant is achieved by changing only the number of heat exchanger tubes. Then the parameters shown in Table 5-11 are assumed to remain constant. The number of tubes and the areas on either side of a HTSE heat exchanger are shown in Table 5-12 as derived by applying the scaling factor to the values of these same parameters in the once-through design. The energy capacitances are assumed to scale similarly. Values are given in Table 5-13.

The values of the time constants for each of the superheater, boiler, and condenser in the HTSE plant are given in Table 5-14. These values are from the once-through steam generator in [Vilim 2001]. It has been assumed that in adjusting the areas from once-through to HTSE the mass of coolant and structure and the flowrates change by the same factor. This will be true when the flowrates scale proportionally with power which would be the case if the log mean temperature difference remains unchanged. Since this is not exactly the case the time constant values from the once-through unit provide only approximate values.

The representative time constant and energy capacitance finally used for each HTSE component was obtained as follows. Identified in Table 5-13 in bold is the energy capacitance with the largest value among the four energy capacitances for each component. Note that each value is at least twice as big as the next largest value. To the first order then the time constant of the associated capacitance dominates. These time constants are taken as representative of the components and are shown in 5-14 in bold. The bolded values are shown reproduced in summary in Table 5-22.

Table 5-10 Area Factor for Scaling from 300 MWt Oconee Once-Through Steam Generator to HTE Water Heat Exchangers

| Region-to-Component Correspondence | | $Q$ (MWt) | | $T_{hi}$ (C) | | $T_{ho}$ (C) | | $T_{ci}$ (C) | | $T_{co}$ (C) | | $\Delta T$ (C) | | | $\frac{A_{HTE}}{A_{OT}}$ |
|---|---|---|---|---|---|---|---|---|---|---|---|---|---|---|---|
| OT Region | HTE Component | OT[b] | HTE[c] | OT | HTE | OT | HTE | OT | HTE | OT | HTE | Eq.() | OT | HTE | |
| Subcooled | Condenser[a] | 16 | 15.4 | 303 | 304 | 293 | 68 | 266 | 21 | 286 | 182 | 18a | 21 | 79 | 0.26 |
| Two-Phase | Boiler | 244 | 43.4 | 452 | 500 | 303 | 339 | 286 | 257 | 286 | 257 | 19a | 65 | 148 | 0.078 |
| Superheated | HX1 | 40 | 26 | 476 | 989 | 452 | 540 | 286 | 257 | 347 | 742 | 18a | 147 | 264 | 0.36 |

[a] Vapor condensing on hot side is small part of total heat load so hot side behaves very nearly as a single phase coolant
[b] [Vilim 2001]
[c] Table 4-8

Table 5-11 Dimensions Preserved in Scaling from Once-Through Steam Generator to HTE Water Heat Exchangers

| Parameter | Value [Vilim 2001] |
|---|---|
| Tube Length (m) | |
| Subcooled/Condenser | 1.14 |
| Two-Phase/Boiler | 0.86 |
| Superheater/HX1 | 1.00 |
| Tube Outside Diameter (m) | 1.67E-02 |
| Tube Inside Diameter (m) | 1.27E-02 |
| Tube Pitch-to-Diameter ratio | 1.355 |
| Shell Thickness | 2.0E-02 |

Table 5-12 HTE Water Heat Exchanger Dimensions Scaled from 300 MWt STAR-LM Once-Through Steam Generator

| Water Phase Region-to-Component Correspondence | | Number of Tubes | | Flow Area on Water Side ($m^2$) | | Flow Area on Non-Water Side ($m^2$)* | |
|---|---|---|---|---|---|---|---|
| STAR-LM Region | HTE Component | STAR-LM | HTE | STAR-LM | HTE | STAR-LM | HTE |
| Subcooled | Condenser | 26720 | 6900 | 5.99 | 1.6 | 3.39 | 0.88 |
| Two-Phase | Boiler | 26720 | 2100 | 5.99 | 0.47 | 3.39 | 0.26 |
| Superheated | HX1 | 26720 | 9600 | 5.99 | 2.2 | 3.39 | 1.2 |

* Based on coolant with specific heat and heat transfer properties of PbBi

Table 5-13 HTE Water Heat Exchanger Energy Capacitances Scaled from 300 MWt STAR-LM Once-Through Steam Generator

| Water Phase Region-to-Component Correspondence | | Energy Capacitance of Shell Structure on Water Side (MJ/C) | | Energy Capacitance of Tube Structure on Non-Water Side (MJ/C) | | Energy Capacitance of Water in Contact with Shell (MJ/C) | | Energy Capacitance of Coolant in Contact with Tube (MJ/C)* | |
|---|---|---|---|---|---|---|---|---|---|
| STAR-LM Region | HTE Component | STAR-LM | HTE | STAR-LM | HTE | STAR-LM | HE | STAR-LM | HTE |
| Subcooled | Condenser | 7 | 1.8 | 14 | 3.6 | 27 | **7.0** | 6 | 1.6 |
| Two-Phase | Boiler | 5 | 0.40 | 11 | 0.86 | 29 | **2.3** | 4 | 0.31 |
| Superheated | HX1 | 6 | 2.2 | 12.4 | **4.5** | 1.4 | 0.50 | 5 | 1.8 |

*Based on coolant with specific heat and heat transfer properties of PbBi

Table 5-14 HTE Water Heat Exchanger Time Constants from 300 MWt STAR-LM Once-Through Steam Generator

| | Shell Structure (s) | Tube Structure (s) | Water in Contact with Shell (s) | Coolant in Contact with Tube* (s) |
|---|---|---|---|---|
| Condenser | 179 | 14 | **30** | 0.4 |
| Boiler | 42 | 1.8 | **20** | 0.4 |
| HX1 | 417 | **35** | 1.3 | 0.4 |

*Based on coolant with specific heat and heat transfer properties of PbBi

### 5.1.4 Reactor Core

The thermal response behavior of the VHTR core is represented by the model for heat transfer of Section 3.4.1. This model assumes the annular unit cell shown in Figure 3-3. Two types of calculations were performed. The first calculation estimates the thermal time constant and the energy capacitance of the core. It is based on the values of unit cell geometry parameters calculated from design data in Table 5-15. The calculation of heat transfer coefficient from solid to coolant is then calculated in Table 5-16. From this Table 5-17 shows the calculation of a core thermal time constant of 9.5 s and an active core region energy capacitance of 200 MJ/C. These values are reproduced in Table 5-22.

The second calculation of core thermal response is that performed in the GAS-PASS/H dynamic simulations described in Section 5.5.2. The code solves the dynamic fuel pin model of Section 3.4.1. The data input to that calculation are taken from Tables 5-15 and 5-16.

The neutronic response of the VHTR core is represented by the models for reactivity feedback of Section 3.4.2. Two types of calculations were performed. The first calculation estimates the neutronic time constant of the core based on the model of Section 3.4.2.7. This calculation requires an estimate for the integral feedback parameters A, B, and C which in turn require estimates for the differential worth of control rods and for individual reactivity coefficients. The differential rod worth is calculated in Table 5-18 and control rod reactivity coefficients in Table 5-19. The remaining reactivity coefficients and the integral feedback parameters are calculated in Table 5-20. Given these values and a one-group precursor half life of $\lambda = 0.1\ s^{-1}$ and $A+B = -2.7$ *$* from Table 5-20, the long term time constant for core power is 3.7 s. This value is reproduced in Table 5-22.

The second calculation of reactivity feedback is that performed in the GAS-PASS/H dynamic simulations described in Section 5.5.2. The code solves the six-group point kinetics equations for the core power using the expression for net reactivity of Section 3.4.2.5. The values for individual reactivity coefficients are taken from Tables 5-19 and 5-20.

Table 5-15 Values of Design Parameters for Annular Unit-Cell Representation of Fuel Element

| | | | | | | | |
|---|---|---|---|---|---|---|---|
| Coolant | $n_{cl}$ | $A_{cl}\, n_{cl}$ ($m^2$) | $A_{cl}$ ($m^2$) | $r_{cl}$ (m) | $C_{p\text{-}cl}$ (j/kg-C) | $k_{cl}$ (w/m-C) | - |
| | 106 | $102\,\frac{\pi}{4}\,0.016^2 = 0.022$ | 2.1E-04 | 26E-03 | 5200 | 0.37 | |
| Graphite | - | $A_{gr}\, n_{cl}$ ($m^2$) | $A_{gr}$ ($m^2$) | $r_{gr}$ (m) | $C_{p\text{-}gr}$ (j/kg-C) | $k_{gr}$ (w/m-C) | $\rho_{gr}$ ($kg/m^3$) |
| | | $\sqrt{3}(0.360)^2$ -0.022-0.027=0.175 | 1.7E-03 | 25E-03 | 1100 | 80 | 1,740 |
| Fuel | - | $A_f\, n_{cl}$ ($m^2$) | $A_f$ ($m^2$) | $r_f$ (m) | $C_{p\text{-}f}$ (j/kg-C) | $k_f$ (w/m-C) | $\rho_f$ ($kg/m^3$) |
| | | $210\,\frac{\pi}{4}\,0.0127^2 = 0.027$ | 2.5E-04 | 8.9E-03 | 160 ($Cp_{UC_2} \sim Cp_{UC}$) | 20 (UC) | 13,600 |

Table 5-16 Values of Design Parameters for Coolant Channel in Fuel Element

| | | | | |
|---|---|---|---|---|
| Coolant Mass Flow Rate | Number of Coolant Holes per Fuel Element | Number of Fuel Element Columns | Coolant Mass Flow Rate in Fueled Elements (kg/s) | Coolant Mass Flow Rate per Coolant Channel (kg/s) |
| | 106 | 72+30=102 | 288*0.85=244 | 0.023 |
| Coolant Heat Transfer Coefficient | $(Re)_{He}$ | $(Pr)_{He}$ | $D_{cl}$ (m) | $h_{cl} = \frac{k_{He}}{D_{cl}} 0.023\ \mathrm{Re}^{0.8}\ \mathrm{Pr}^{0.3}$ ($W/m^2$-C) |
| | 41,000 | -1 | 0.016 (coolant channel diameter) | 2600 |

Table 5-17 Thermal Time Constant and Capacitance of Fuel Element as Represented by Solid Cylinder

| | | | | |
|---|---|---|---|---|
| Volume per Fuel Element | Exterior Volume ($m^3$) | Coolant Volume ($m^3$) | Fuel Matrix Volume, ($m^3$) | Graphite Volume, ($m^3$) |
| | $\sqrt{3}(0.360)^2\ 0.79 = 0.177$ | $108 \cdot 0.79 \cdot \frac{\pi}{4} \cdot 0.016^2 = 0.017$ | $210 \cdot 0.79 \cdot \frac{\pi}{4} \cdot 0.0127^2 = 0.021$ | 0.177-0.017-0.021 = 0.139 |
| Volume per Coolant Hole | Coolant Volume, $V_{cl}$ ($m^3$) | Fuel Matrix Volume, $V_f$ ($m^3$) | Graphite Volume, $V_c$ ($m^3$) | |
| | 0.017/108 = 0.157e-3 | 0.021/108 = 0.194e-3 | 0.139/108 = 1.29e-3 | |
| Mass per Fuel Element | $UO_2$ Mass (Kg) | $UC_2$ Mass (Kg) | C Mass (Kg) | |
| | ~2350/720 = 3.26 | ~2350/720 = 3.26 | 0.139·1740 = 242 | |
| Mass per Coolant Hole | $m_{UO_2}$ (Kg) | $m_{UC_2}$ (Kg) | $m_C$ (Kg) | |
| | 3.26/108 = 0.030 | 3.26/108 = 0.030 | 242/108 = 2.24 | |
| Density | $\rho_{UO_2}\ (Kg/m^3)$ | $\rho_{UC_2} \sim \rho_{UC}\ (Kg/m^3)$ | $\rho_C\ (Kg/m^3)$ | |
| | 11,000 | 13,600 | 1,740 | |
| Specific Heat | $Cp_{UO_2}$ (J/Kg-c) | $Cp_{UC_2} \sim Cp_{UC}$ (J/Kg-C) | $Cp_C$ (J/Kg-C) | |
| | 300 | 160 | 1100 | |
| Conductivity | $k_C$ (W/m-K) | $k_{He}$ (W/m-K) | | |
| | 80 | 0.37 | | |
| Thermal Capacitance per Coolant Hole | $(mC_\rho)_{UO_2} + (mC_\rho)_{UC_2} + (mC_\rho)_C$ (J/°C) | | | |
| | 0.03·300+0.03·160+2.24·1100 = 2500 | | | |
| Equivalent Radius of Solid per Coolant Hole | L (m) | $V = V_C + V_f$ ($m^3$) | $r = \left(\frac{V}{\pi L}\right)^{1/2}$ (m) | |
| | 0.79 | (1.29+0.194)e-3 = 1.48e-3 | 0.024 | |

Table 5-17 Thermal Time Constant and Capacitance of Fuel Element as Represented by Solid Cylinder (cont'd)

| | | | | |
|---|---|---|---|---|
| Coolant Heat Transfer Coefficient | $(Re)_{He}$ | $(Pr)_{He}$ | $D_{cl}$ (m) | $h_{cl} = \frac{k_{He}}{D_{cl}} 0.023\ \mathrm{Re}^{0.8}\ \mathrm{Pr}^{0.3}$ ($W/m^2$-C) |
| | 41,000 | -1 | 0.016 | 2600 |
| Effective Heat Transfer Coefficient (J/s-m-C) | $h = \left( \frac{r}{4k_C} + \frac{1}{h_{cl}} \right)^{-1}$ | | | |
| | $\left( \frac{0.024}{4.80} + \frac{1}{2600} \right)^{-1} = 2200$ | | | |
| Fuel Element Time Constant (s) | $\tau = \frac{\rho V C_p}{2\pi rhL}$, (s) Eq.(x) | | | |
| | $\frac{2500}{2\pi \cdot 0.024 \cdot 2200 \cdot 0.79} = 9.5$ | | | |
| Active Core Energy Capacitance (J/C) | $\left[ \left( mC_\rho \right)_{UO_2} + \left( mC_\rho \right)_{UC_2} + \left( mC_\rho \right)_C \right] \cdot N_{holes} \cdot N_{elements}$ | | | |
| | $2500 \cdot 108 \cdot 720 = 200e6$ | | | |

Table 5-18 Upper Bound for Differential Worth of Operating Control Rods for GT-MHR

| | |
|---|---|
| Number of Operating Control Rods[a] i.e., outer neutron control | 36 |
| Upper limit on worth per rod[b] ($) | 0.5 |
| Absorber length of Operating Control Rod[c] (in/m) | 229/5.8 |
| Worth per absorber per unit absorber length ($/m) | 0.5/5.8=0.086 |
| Combined worth of Operating Control Rods per unit absorber length ($/m) | 0.086(36) = 3.1 |

[a] Startup control rods are withdrawn before criticality: p.4-5 and p. 4-12 of [Shenoy 1996].
Operating control rods are inserted to varying heights during operation: p.4-22 of [Shenoy 1996].
[b] Each control rod has its own independent drive: p.4-26 of [Shenoy 1996]. Any single drive, for safety reasons, should be limited to less then one dollar.
[c] Figs. 4.1-12, 4.1-13, and 4.2-2 [Shenoy 1996]. Scaled from these figures.

Table 5-19 Deviation of Control Rod Reactivity Coefficients for VHTR

| | |
|---|---|
| Operating Control Rods -Vessel | 437·2.54e-2 =11.1 |
| Length, L (m) (hot duct to top of core) | |
| Steel coefficient of thermal expansion, β (m/m/C) | 1.5e-5 |
| Differential worth, dρ/dL ($/m) [Table 5-18] | 3.1 |
| $\alpha_{cr\text{-}v}$ [Eq. (3-67)] ($/°C) | 11.1·1.5e-5 ·3.1 = 5.2e-4 |
| Operating Control Rods - Moderator | 7.93 |
| Length[a], L (m) (active core height), | |
| Graphite coefficient of thermal expansion, β (m/m/C) | 0.3e-5 |
| Differential worth, dρ/dL ($/m) [Table 5-18] | 3.1 |
| $\alpha_{cr\text{-}m}$ [Eq. (3-67)] ($/°C) | -7.93·0.3e-5 ·3.1 = -0.74e-4 |

[a] p.30 of [MacDonald 2003]

Table 5-20 Integral Reactivity Coefficients for VHTR

| | |
|---|---|
| Operating Control Rods - Vessel, $\alpha_{cr\text{-}v}$ (\$/°C) | [0,+5.2e-4][a], mean=2.6e-04 |
| Operating Control Rods - Moderator, $\alpha_{cr\text{-}m}$ (\$/°C) | -0.74e-4 |
| Moderator, $\alpha_m$ (dk/dT) @ 770° C [b] (Fig. 37 [MacDonald 2003] ) | [-1.0e-5, +4.0e-5] |
| $\alpha_m$ (\$/°C) | [-1.67e-3, +6.67e-3], mean=2.5e-03 |
| Fuel, $\alpha_f$ (dk/dT) @ 820° C [b] (Fig. 35 [MacDonald] ) | [-5.5e-5, -4.4e-5] |
| $\alpha_f$ (\$/°C) | [-9.2e-3, -7.3e-3], mean= - 8.25e-03 |
| Average moderator temperature rise[b], $\Delta T_{m\text{-}100}$ (°C) | 100 |
| Average fuel temperature rise[b], $\Delta T_{f\text{-}100}$ (°C) | 50 |
| Coolant temperature rise, $\Delta T_{c\text{-}100}$ (°C) | 510 |
| $A = \alpha_f \ (\Delta T_{m\text{-}100} + \Delta T_{f\text{-}100})$, (\$) | - 1.2 |
| $B = (\alpha_m + \alpha_{cr\text{-}m} + \alpha_f)/2 * \Delta T_{c\text{-}100}$, (\$) | - 1.5 [d] |
| $C = \alpha_{cr\text{-}v} + \alpha_m + \alpha_{cr\text{-}m} + \alpha_f$ | -5.6e-03 [d] |
| A+B, (\$) | - 2.7 [d] |
| $1 - \frac{C\Delta T_{c-100} / B}{\frac{A}{B} + 1}$ | - 0.042 [d] |
| $C\Delta T_{c-100} / B$ | 0.90 [d] |
| $\frac{A}{B}$ | 0.83 [d] |

[a]Vessel time constant is large at six inch thickness. Range covers time that varies from instantaneous to infinite.
[b]Average moderator and fuel temperatures from Table 11 of [MacDonald 2003].
[c]$\beta_{eff} \sim 6x10^{-3}$.
[d]based on mean values

### 5.1.5 Process Heat Pipes

Dimensions for the pipes to and from the HTSE process are for FLINAK and a distance of 90 m.[Lillo 2005] Data is given in Table 5-21. Time constant and energy capacitance values calculated there are reproduced in Table 5-22.

Table 5-21 Time Constants and Energy Capacitances of Coolant and Wall of Pipes to/from HTE Plant. FLINAK and separate hot/cold legs.

| Pipe Dimensions | Length, L (m) | Inner Radius, $r_i$ (m) | Outer Radius, $r_o$ (m) | Flowrate, w (kg/s) | Velocity, v (m/s) | | |
|---|---|---|---|---|---|---|---|
| | 90 | 0.065 | 0.079 | 133 | 5.3 | | |
| Coolant | $\mu$ (Pa-s) | $C_p$ (J/C-kg) | $k$ (W/m-C) | $\rho$ ($kg/m^3$) | $Re$ | $Pr$ | $h_{cl} = \frac{k_{He}}{D_{cl}} 0.023\ \mathrm{Re}^{0.8}\ \mathrm{Pr}^{0.3}$ ($W/m^2$-C) |
| | 1.62E-03 | 1905 | 0.8 | 1880 | 8.0E05 | 3.9 | 1.1E04 |
| Structure | $k$ (W/m-C) | $C_p$ (J/C-kg) | $\rho$ ($kg/m^3$) | | | | |
| | 25 | 500 | 8000 | | | | |
| $\frac{1}{h} = \frac{\Delta t}{2k} + \frac{1}{h_{cl}}$ ($W/m^2$-C) | 2700 | | | | | | |
| Time Constants and Energy Capacitances | $\tau_s = \left(\frac{\rho \Delta t C_p}{h}\right)_s$ (s) | $\tau_{cl} = \frac{\left(\rho V C_p\right)_{cl}}{\left(w C_p\right)_{cl} + hA}$ (s) | $\left(\rho V C_p\right)_s$ (MJ/C) | $\left(\rho V C_p\right)_{cl}$ (MJ/C) | | | |
| | 21 | 12 | 2.3 | 4.3 | | | |

### 5.1.6 Overall Plant

Expressions for time constants and energy capacitances were derived in Section 3 and evaluated for the major components in Section 5.1. The results are summarized in Table 5-22 and are used in the following subsections to draw some preliminary conclusions.

Some simple observations are made. The reactor and PCU vessel walls have very large thermal capacitances (1000 MJ/C) but the time constant for these components as they interact with the helium coolant is almost an hour. Thus, upset events of the order of several minutes, these capacitances will not be particularly active. However, during startup this capacitance will be important. It will not be important for operational transients since the vessel walls are maintained at constant temperature.

The overall time response of the contents of the reactor vessel is largely a function of the fuel. The neutronics are essentially quasi-static compared to the fuel (3.7 s versus 9.5 s) while the fuel energy capacitance (200 MJ/C) is large. Judging from the physical space occupied by the fuel in the reactor vessel, it would appear to be greater than all other structure energy capacitances that are faster than a few tens of seconds. The helium coolant is insignificant (4.7 MJ/C) compared to the fuel.

In the HTE plant the energy capacitance of the electrolytic cells (270 MJ/C) is almost a factor of ten greater than all the other components combined (~30 MJ/C). The time constant (206 s) is also roughly ten times greater than the other components (12-35 s). However, since the electrolytic cells are essentially downstream of the process heat components of the HTE this heat capacity will have little effect in dampening a transient there. It does mean that rapid transients (seconds) in that part of the plant will be muted in their impact on electrolytic cell temperature. Essentially, with the process heat components operating at a power level of 50 MW small transients will be limited in the rates of temperature change they can induce in the electrolytic cells. Similarly, with the electrolysis process depositing only about 10 MW of thermal energy in the cells, transients in the electric generating part of the plant will result in limited rates of temperature change in the cells.

## 5.2 Plant Startup

A preliminary procedure for bringing the combined plant up to full power from cold subcritical is given in Table 5-23.

The time taken to reach full power is limited by the reactor power input to the combined plant and the heat capacity of the combined plant. Table 5-22 suggests that the total heat capacity is of the order 3000 MJ/C. Suppose the reactor power is raised linearly from 0 to 600 MWt and half of the heat is rejected to the heat sink. If the plant is at room temperature and on average is raised to the core mid-plane temperature at full power, then the time taken is

$$3000E06(J/C) * 700 (C) / (600E6(J/s) * 0.5 * 0.5) = 14{,}000 \text{ s}$$

or about four hours.

Table 5-22 Summary of Thermal Time Constants and Capacitances

| | Time Constant (s) | Energy Capacitance (MJ/°C) | Ref. | Notes |
|---|---|---|---|---|
| **Reactor Vessel** | | | | |
| Active Core | | | | |
| Fuel Elements | 9.5 | 200 | | |
| Neutronics | 3.7 | - | | |
| He Coolant | 2.8[a] | 4.7 | | Assumes 0.2 void fraction |
| Internals | unknown | unknown | | |
| Wall | 4000 | 1000 | | < 500 C |
| **Intermediate System** | | | | |
| IHX | 0.28 | 27 | | |
| Flow Paths | unknown | unknown | | |
| **Power Conversion Unit** | | | | |
| Turbine | - | 8.0[b] | | |
| Recuperator | 1.9 | 95 | | |
| Vessel Wall | 2300 | 1000 | | < 500 C |
| Coolers | - | - | | < 200 C |
| Compressors | - | - | | < 200 C |
| **HTE Plant** | | | | |
| HTLHX | 0.96 | 2.8 | | |
| Outbound Pipe | | | | |
| Pipe Wall | 21 | 2.3 | | 100 m; molten salt |
| Coolant | 12 | 4.3 | | 100 m; molten salt |
| Inbound Pipe | | | | |
| Pipe Wall | 21 | 2.3 | | 100 m; molten salt |
| Coolant | 12 | 4.3 | | 100 m; molten salt |
| Condenser | 30 | 7 | | |
| Boiler | 20 | 2.3 | | |
| Superheater HX1 | 35 | 4.5 | | |
| Electrolytic Cells | 206 | 270 | | |

[a] Mixing [b] Based on mass of rotor and static structure estimated to be 16,000 kg

However, the time rate of change of temperature in thick structures such as the wall of the reactor and PCU vessels may have to be limited to achieve acceptable thermal stresses. There may be a similar consideration for the pressure boundary for the electrolytic cells which operate at high temperature and pressure. Thus, a startup time of four hours is a lower bound.

Table 5-23 Preliminary Startup Procedure for Representative VHTR/HTE Plant Configuration

| Combined Plant Operating Mode | Sequence of Control Actions | Terminal condition |
|---|---|---|
| Reactor to Hot Critical | - | Subcritical core, cold and atmospheric pressure primary system |
| | Add inventory | Subcritical core, cold and uniform partially pressurized primary system |
| | Turning gear on | Subcritical core, hot and non-uniform partially pressurized primary system |
| | Add rod reactivity | Critical core, hot and non-uniform partially pressurized primary system |
| Ascend to House Electric Load | Add rod reactivity, turn on coolers, decouple turning gear | Plant self-sustaining as a heat engine |
| | Add rod reactivity | Increase turbomachine speed to match grid frequency |
| | Synchronize to grid and raise power to equal house load | Reactor at about 3 % load |
| | Turn on molten salt heaters | Thawed hydrogen plant heat transport loop |
| Ascend to House Thermal Load | Startup PH and SHX1 compressors | Two-phase region in boiler |
| | Increase reactor power, increase flow of PH and SHX1 compressors, turn on water pump | Saturated steam delivered to electrolyzer |
| Ascend to Bottom of Operating Range | Startup SHX2 compressor | Superheated steam delivered to electrolyzer |
| | Increase reactor power. Deliver electric power to electrolyzer. | Electrolyzer at temperature at bottom of operating range |
| Ascend to Full Power | Follow combined plant load schedule to full power condition: Inventory Control for reactor, Flowrate Control for HTE plant | HTE plant at full power hydrogen production |

## 5.3 Step Change in Hydrogen Production

### 5.3.1 Electrolyzer Response

The electrolyzer output quantities (species concentration, structure temperatures, and temperatures of gas streams) respond to changes in cell inlet conditions (current and inlet temperature) to the first order on a time scale given by the cell time constant. An expression for the time constant is given in Section 3.1 and an estimate for its value is given in Table 5-4. One sees that it would take about ten minutes for the cell to reach a new equilibrium state if equilibrium conditions were defined as being reached three time constants after a step change in input conditions. However, this is the inherent response of the cell. The adjustment of the output conditions to a change in inputs could be accelerated through manipulation of the inputs by a controller.

### 5.3.2 HTSE Plant Response

In addition to partial power steady-state operation, a power reactor is typically designed to be able to meet an instantaneous change in generator power of ten percent. The initial and final states are given by the load schedule. However, in the interim, dynamics are excited and the plant deviates from equilibrium. The transient behavior is obtained from a dynamic simulation. However, a measure of the deviation can be estimated using the method of Section 2.2.

The load change considered is a ten percent step increase in hydrogen demand for the HTSE plant of Figure 4-3. It is assumed that the reactants from Compressor 1and Pump 2 up to the Cell 11 inlet and the products from the Cell 1 output to Condenser 3 increase by this amount. All other flowrates in the combined plant and the electric power to the cell are assumed to remain constant. Of interest is the rate at which temperatures in the HTE plant change before the control system acts to bring control variables into agreement with the load schedule for the new hydrogen production level.

Inspection of Figure 4-3 reveals that the HTSE equipment components containing either water and/or cell products are all tightly coupled thermally to each other. The two recuperating heat exchangers are responsible. An approximate estimate for the rate of temperature change throughout these components (condenser, boiler, HX1, HX2, cell, and turbine) is obtained from Eq. (2-7). Before the load change the thermal power provided by PHX1 and PHX2 is 50 MWt while the thermal output from the electrolyzer is about 10 MWt. The energy capacitance from Table 5-22 is 270 MJ/C for the electrolyzer and about 30 MJ/C for the other components. The temperature rates of change amongst the components for a ten percent change in power will from Eq. (2-7) range from $0.02^{o}$ C/s (=0.1*60/300) to $0.17^{o}$ C/s (=0.1*50/30).

In summary, the rate of temperature change in each component will be limited to less than $0.2^{o}$ C/s. This is about a factor of five below rates ($1^{o}$ C/s) that might lead to accumulated fatigue at the tube sheet in a large (hundreds of MW) tube and shell heat exchanger operating at $500^{o}$ C. The HTSE heat exchangers are smaller (tens of MW) so temperature rates of change would have to be greater yet than $1^{o}$ C/s to create a fatigue problem. The exception may, however, be HX2 which operates at an outlet temperature of $850^{o}$ C.

## 5.4 Reactor Trip

A reactor trip would be followed by an automatic runback in primary flowrate to avoid thermal shock to the hot side components in the primary loop and intermediate loop. The generator would automatically disconnect from the grid since it would not be able to meet grid demand. The result is that the electrical power to the electrolyzer and the thermal power to the HTE plant would drop to near zero. In the scenario envisioned the molten salt line to the HTE plant would no longer be heated but would still be in thermal contact with the boiler water inventory. Unless isolated, the water would continue to boil draining heat from the lines possibly causing the salt to freeze.

### 5.4.1 Molten Salt Process Heat Loop Response

The issue is how much margin to freezing would remain if the boiler were not isolated? A simple calculation provides some insight. For the boiler volume computed from data in Tables 5-11 and 5-12 and an assumed void fraction of 0.667, the resulting inventory is capable of removing approximately 300 MJ of energy through the latent heat of vaporization. Based on an initial sizing of the boiler the latent heat of vaporization of the water inventory is approximately 300 MJ. (Note this differs from the value in Table 5-22 which applies only about an operating point.) Table 5-22 shows the molten salt lines represent about 14 MJ/C of heat capacity. Thus, the water inventory could lower the average temperature of the molten salt lines by about $20^{o}$ C, probably not enough to freeze all the salt. Depending on the nature of the gravity head in the molten salt line, local freezing near the boiler might be averted by maintaining natural circulation in the molten salt circuit with the boiler acting as a heat sink.

## 5.5 Loss of HTSE Heat Sink

### 5.5.1 Reactor Response

General stability criteria for an at-power core coupled to a heat sink were developed in Section 2-5. Essentially three criteria must be met, one of which relates the perturbation to core outlet temperature resulting from a temperature perturbation at the inlet. A necessary condition for the reactor to tend toward stable operation is that the core temperature feedback processes attenuate the effect of an inlet temperature perturbation on the outlet temperature of the core. Eq. (2-12) provides an expression for the degree of attenuation.

The magnitude and sign of the attenuation of inlet temperature perturbation was calculated for the VHTR core. The quantity in parenthesis in Eq. (2-12) was evaluated at full power conditions. Table 5-18 presents the estimate for rod differential worth. Normally the Operating Control Rods are inserted into the top of the core to maintain criticality. An increase in vessel temperature causes the rods to be move upward relative to the top of the core adding reactivity. An increase in fuel element temperature causes the core length to increase effectively causing the rods to move further into the core adding negative reactivity. The reactivity coefficients associated with these differential expansions are derived in Table 5-19. The attenuation coefficient of Eq. (2-12) is calculated in Table 5-20. It has a value of -0.042 indicating near complete attenuation at the

outlet of temperature perturbations arising at the inlet. On the basis of this one would expect the VHTR core coupled to a heat source to be very stable with respect to neutronic power.

Another stability assessment was made by comparing the values of two parameters identified in [Depiante 1994] as being important for controlling stability. These parameters and their values appear as the last two entries in Table 5-20. Figure 5-2 shows these values plotted on a stability map taken from [Depiante 1994]. According to this map the core power again is stable with respect to coupling to a heat sink. Note that in Figure 5-2 the x and y axis parameters are the same as the second last and last entries, respectively, in Table 5-20.

These stability criteria are probably of greater significance for coupling to the Sulfur Iodine (SI) plant compared to the HTSE plant. Consider first the case of the HTSE plant. More than 90 percent of the VHTR core thermal power is delivered to the PCU. The coupled neutronic and thermal feedback processes in the core have a combined time constant of about 10 s (Table 5-22) while the transit time from the core outlet through the IHX and through the turbine and recuperator of the PCU and back to the core inlet is estimated to be about 10 s based on an estimated helium volume of 700 $m^3$ and a mass flowrate of 320 kg/s. This comparatively short transit time means the opportunity for out of phase behavior is minimized. While the thermal power delivered to the HTSE plant has a propagation time through the outbound and inbound pipes of the order 25 s (Table 5-22) and thus would tend to promote oscillations, the power is only a few percent of the total core power. Hence, the reactor inlet temperature perturbation introduced through this path will be small and not a strong source of instability. Next consider the SI plant. This heat sink consumes almost all the core thermal power while the propagation time through the outbound and inbound pipes to the hydrogen plant cited above is significantly longer than the 10 s core time constant. Thus, stability issues will be more pronounced for the VHTR coupled to the SI process compared to the HTSE process.

Future work should examine the more general case of reduced primary flowrate to characterize how attenuation represented by Eq. (2-12) is changed. The transit time through the PCU will increase to a value that exceeds the core power time constant violating one of the three stability criteria.

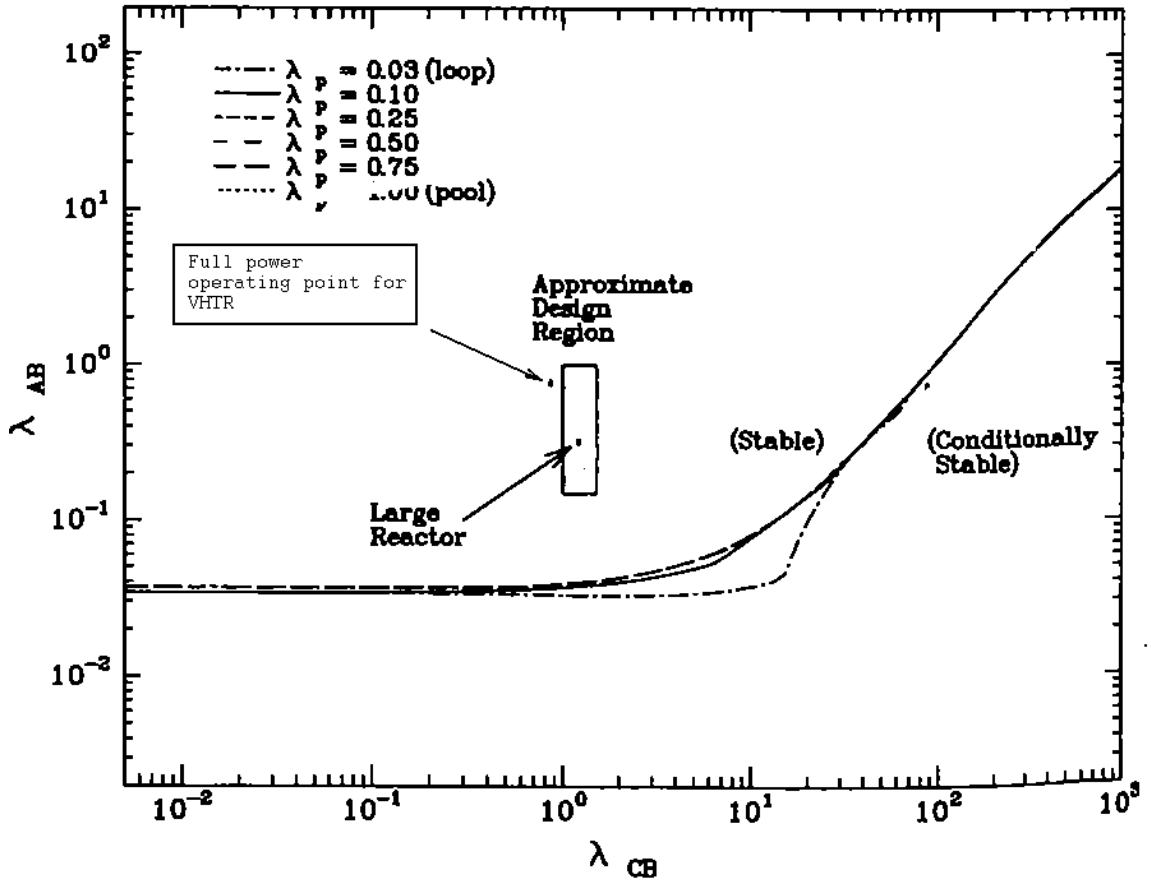


Figure 5-2 Stability Map for Inlet Temperature Perturbations Showing Location of VHTR Core

### 5.5.2 Indirect Cycle Primary System Response

As described earlier the stability of the combined reactor-chemical plant depends on several factors. These include the dependence of core neutronic power on temperature reactivity feedbacks, the coupling of the core to the heat sink via the intermediate heat, and the time for a perturbation in core outlet temperature to propagate back to the inlet to the core. The analysis of the Section 2-5 addressed only temperature feedback, in a quasi-static setting, and the accompanying tendency to either attenuate or amplify the passage of perturbations in reactor inlet temperature through the core. A more complete indication of plant stability for the VHTR-HTSE is obtained by including all three phenomena in a dynamic simulation. This section describes results obtained using the GAS-PASS/H dynamic systems code.[Vilim 2004]

In developing an understanding of the time behavior of the plant the manner in which the time lag is represented in the simulation is important. In the VHTR-HTSE reference design there are three components to the propagation of a temperature front from core outlet to inlet. They are, starting at the reactor outlet,: the circulation time around the primary system, the circulation time out through the IHX and through the PCU and the return back through the IHX, and a similar

circulation path through the IHX but this time through the hydrogen process heat loop. With all three time lags acting simultaneously, the role attributable to each of these paths in the integrated plant behavior is somewhat obscured. A clearer picture is obtained by introducing a simplified representation. A single time lag between the core outlet and inlet captures the essence of all three components. A measure of stability is obtained by varying this parameter and observing the tendency for outlet temperature and power time variations to be naturally damped.

The plant configuration simulated is shown in Figure 5-3. It contains the main features of the closed-loop indirect Brayton cycle of the reference design which are a closed-loop primary system coupled to a heat sink through an intermediate heat exchanger. In the simulation the inlet to the cold side of the heat exchanger is driven by a temperature forcing function used to represent a perturbation that originates in the PCU or HTSE plant. The perturbation upon reaching the heat exchanger passes through it, enters the core, and potentially initiates under-damped oscillations at the reactor outlet. The outlet temperature perturbation makes its way to the core through the three different paths described above. Each has a characteristic time. A single mixing volume between the core outlet and inlet to the hot side of the heat exchanger is used to represent the associated delay.

In addition to the transport time delay, other phenomena important for reactor-heat sink dynamic behavior are included in the simulation. These include 1) the storage of mass and energy in the coolant in the core channels and the hot and cold sides of the intermediate heat exchanger. Data used in the simulation for this heat exchanger are given in Table 5-5. 2) The storage of energy in the fuel and graphite. Data used in the simulation are given in Table 5-15. 3) Reactivity as a function of temperature. Data used in the simulation are given in Table 5-20. 4) A six-group point kinetics model driven by individual temperature feedback components.

Simulations were performed for a near-step increase in temperature at the inlet to the cold side of the intermediate heat exchanger. The forcing function is shown in Figure 5-4. The magnitude of the temperature increase resulted in an asymptotic decrease in core power of 50 MWt without active reactivity addition (i.e. control rod movement) which equals the full power heat input to the HTSE plant. The temperature increase was purposely selected to correspond to a complete loss of the HTSE plant as a heat sink. The results for a 20 s mixing volume time constant appear in Figure 5-5 through 5-9. The coolant, graphite, and fuel average temperature are shown in Figure 5-5. The reactivity components are shown in Figures 5-6. The reactor power appears in Figure 5-7. The outlet temperature of the core and of the mixing volume is shown in Figure 5-8. Figure 5-9 shows the change in core outlet temperature versus change in core inlet temperature. The inherent stability of the reactor is reflected in the change in reactor outlet temperature versus the change in reactor inlet temperature. The reactor response is considered stable if the outlet temperature is damped and in-phase with the inlet temperature.

Propagation of $H_2$ Plant Temperature Disturbance in Combined Plant

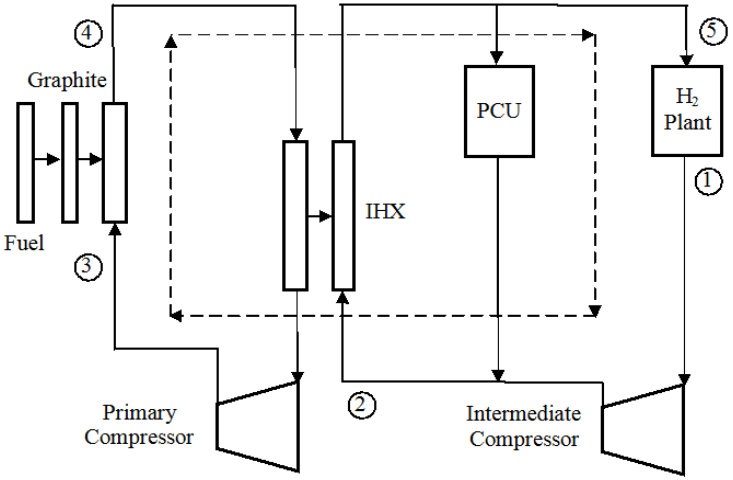


Points along Path of Propagation

① Initial temperature perturbation

② Perturbation enters IHX

③ Perturbation enters core

④ Phased-lagged perturbation exits core

⑤ Perturbation returns to H2 plant

Path Delay with Potential to Create Instability

④ - ⑤ - ① - ② - ③

Canonical Representation of Combined Plant with Surrogate Path Delay

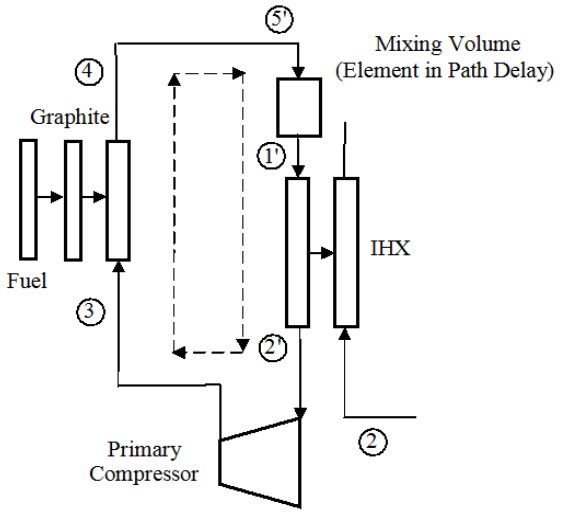


Surrogate Path Delay for Investigation of Stability

④ - ⑤' - ①' - ②' - ③

Figure 5-3 Plant Configurations Appearing in Assessment of Combined-Plant Stability

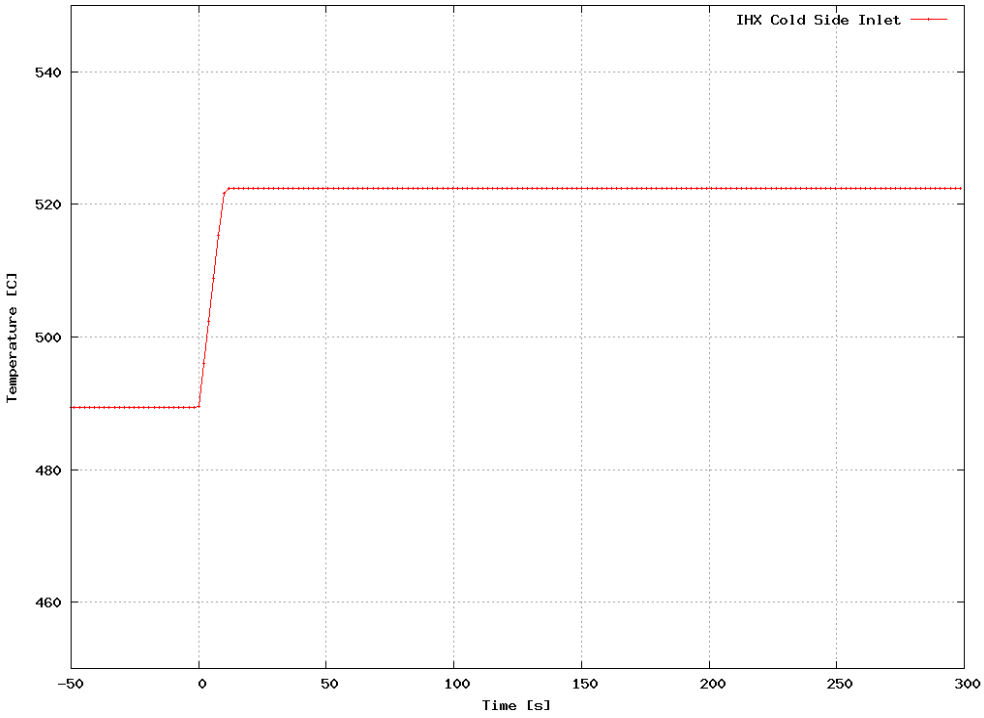


Figure 5-4 Inlet Temperature to Cold Side of IHX – Forcing Function for Stability Investigation

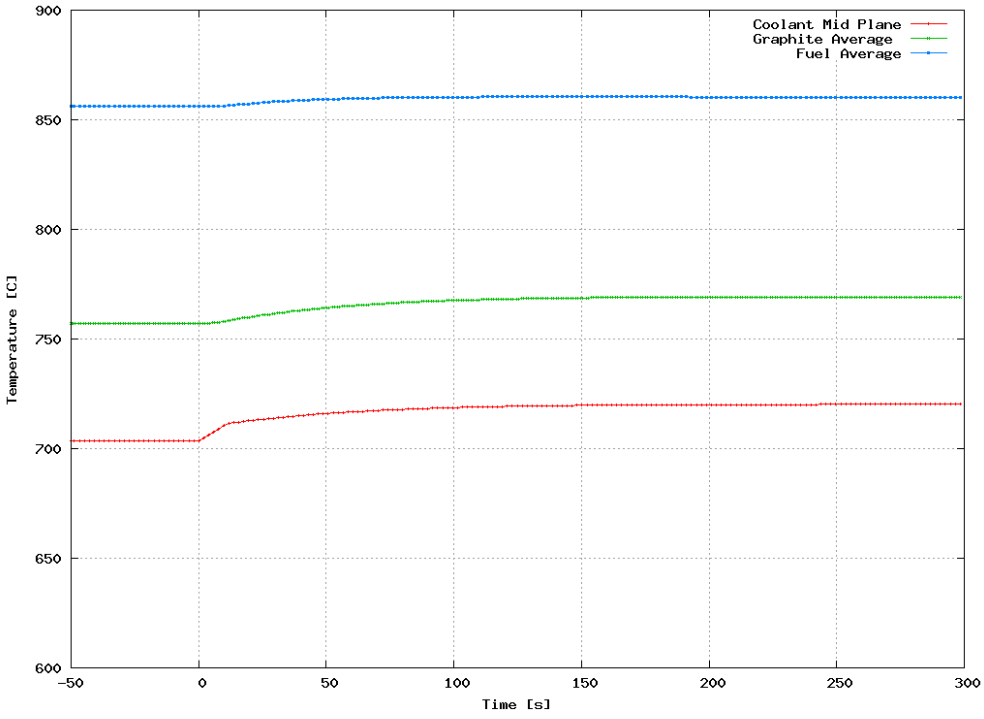


Figure 5-5 Core Temperatures for 20 s Mixing Time Constant

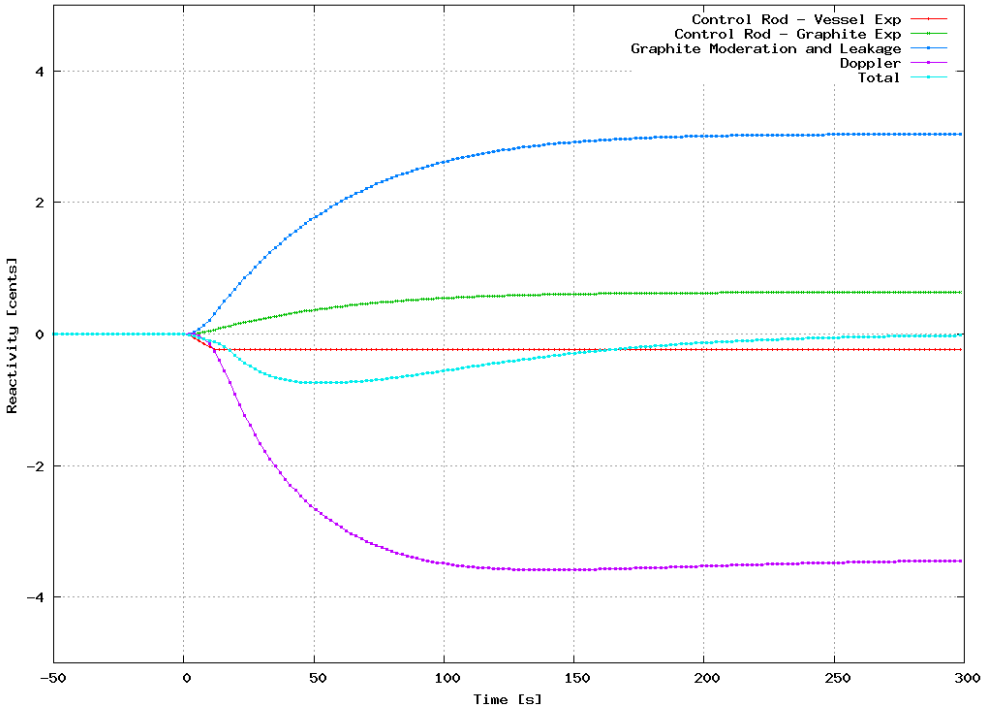


Figure 5-6 Reactivity Components for 20 s Mixing Time Constant

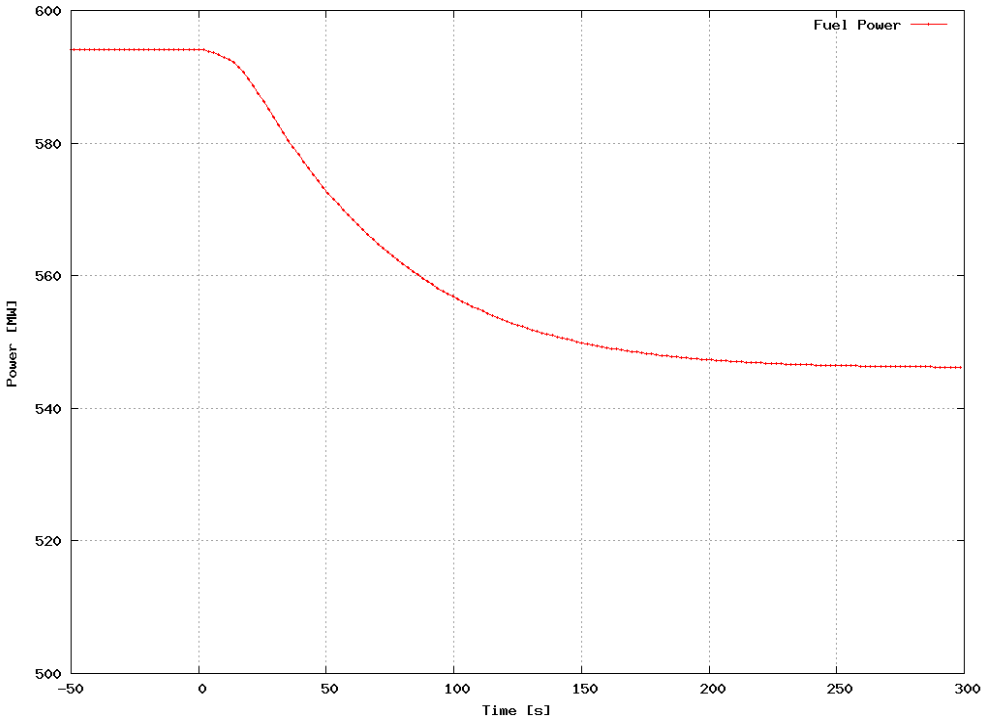


Figure 5-7 Reactor Power for 20 s Mixing Time Constant

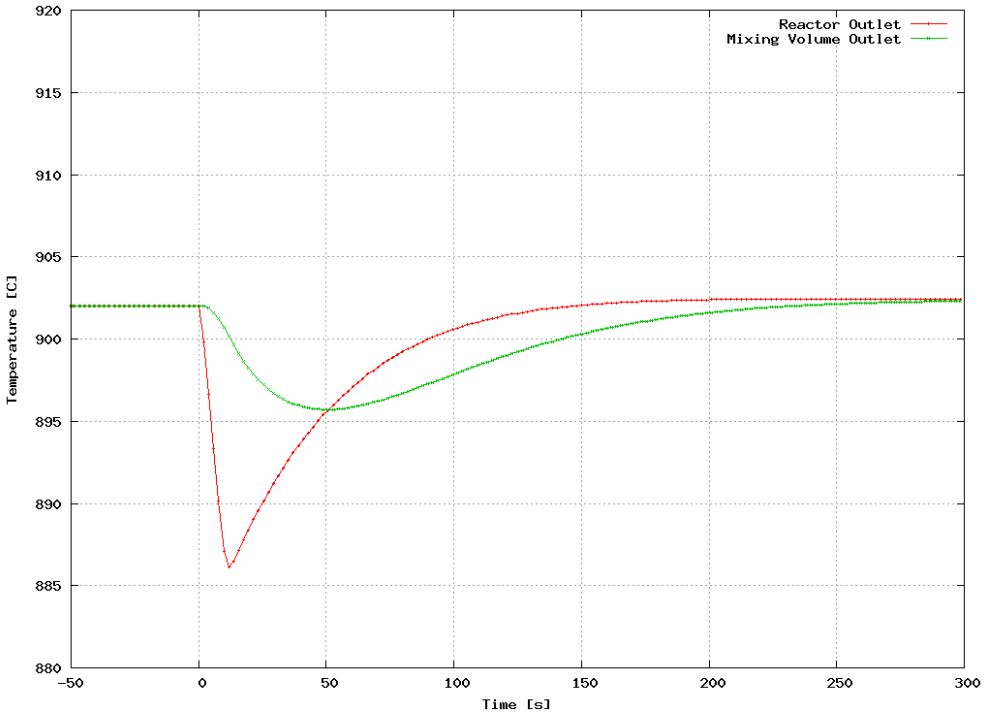


Figure 5-8 Core Outlet and Mixing Volume Outlet Temperatures for 20 s Mixing Time Constant

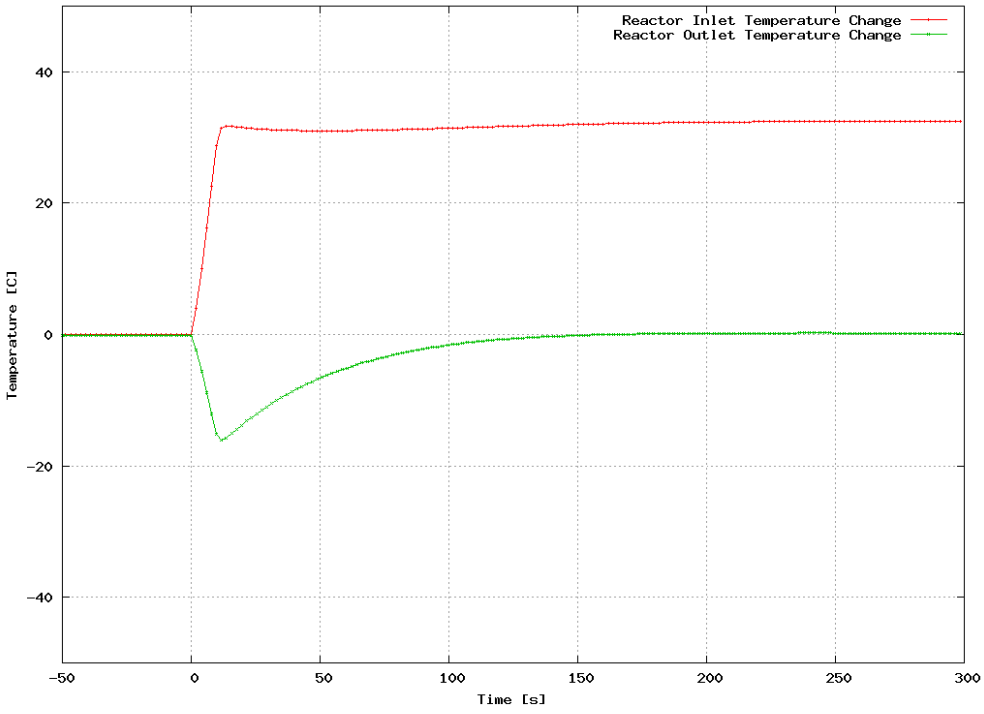


Figure 5-9 Change in Core Inlet and Outlet Temperatures for 20 s Mixing Time Constant

The potential for instability was investigated across a broad range of outlet-to-inlet transport delays. Simulations of the VHTR response to the forcing function in Figure 5-4 were performed for mixing volume time constant values of 5, 50, and 500 s. Figure 5-10 shows the change in core outlet temperature versus change in core inlet temperature for these three values. The corresponding inherent power response (i.e. not control rod motion) appears in Figure 5-11.

The dynamic simulation results indicate temperature perturbations originating in the HTSE plant will not give rise to unstable reactor behavior. Instead, the reactor response is very stable. Figure 5-10 shows that in the long term the reactor outlet temperature reverts back to its original value before a step change in cold side IHX inlet temperature was imposed. In the short term, Figure 5-10 shows the temperature perturbation at the core inlet is attenuated by at least a factor of two in passing through the core and that the resulting perturbation exiting the core is almost completely attenuated by the IHX before return to the core inlet. This is true for delay times of five through 500 seconds. Figure 5-11 shows the core power is essentially unaffected by the size of the delay. Thus, sustained out-of-phase oscillations between core inlet and outlet temperature do not appear likely in the VHTR-HTSE at full power conditions for nominal values of reactivity feedback coefficients. A large Doppler reactivity component, three times greater than next reactivity component per unit temperature, is mainly responsible. Future work should investigate the sensitivity of this result to variation in the values of reactivity feedback parameters and for partial power conditions, particularly at low mass flow rates.

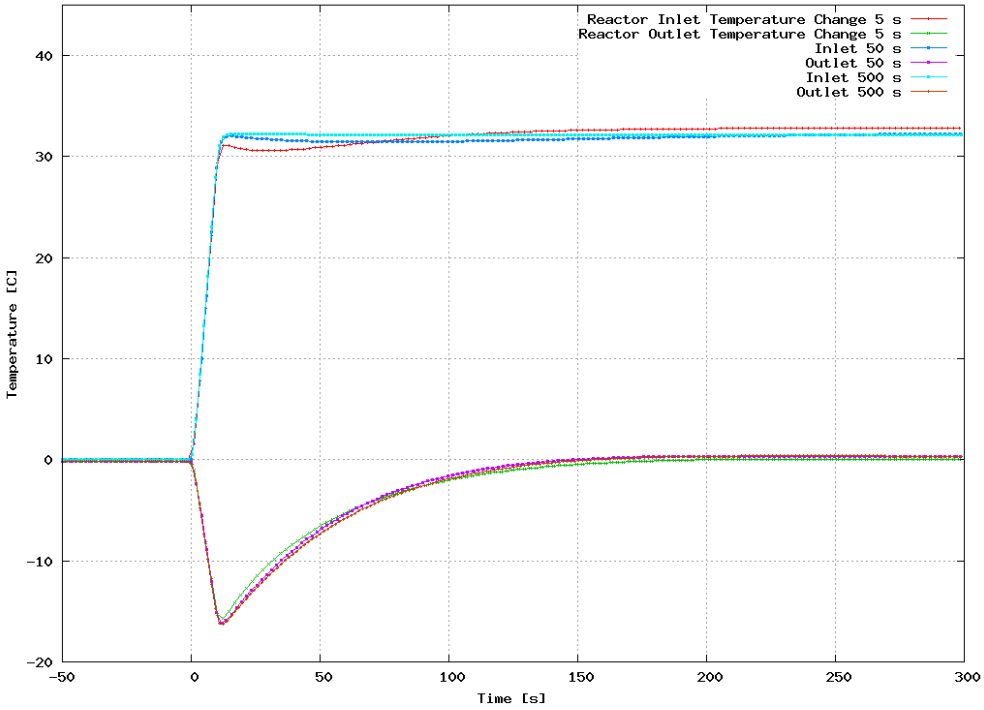


Figure 5-10 Change in Core Inlet and Outlet Temperatures as a Function of Mixing Time Constant

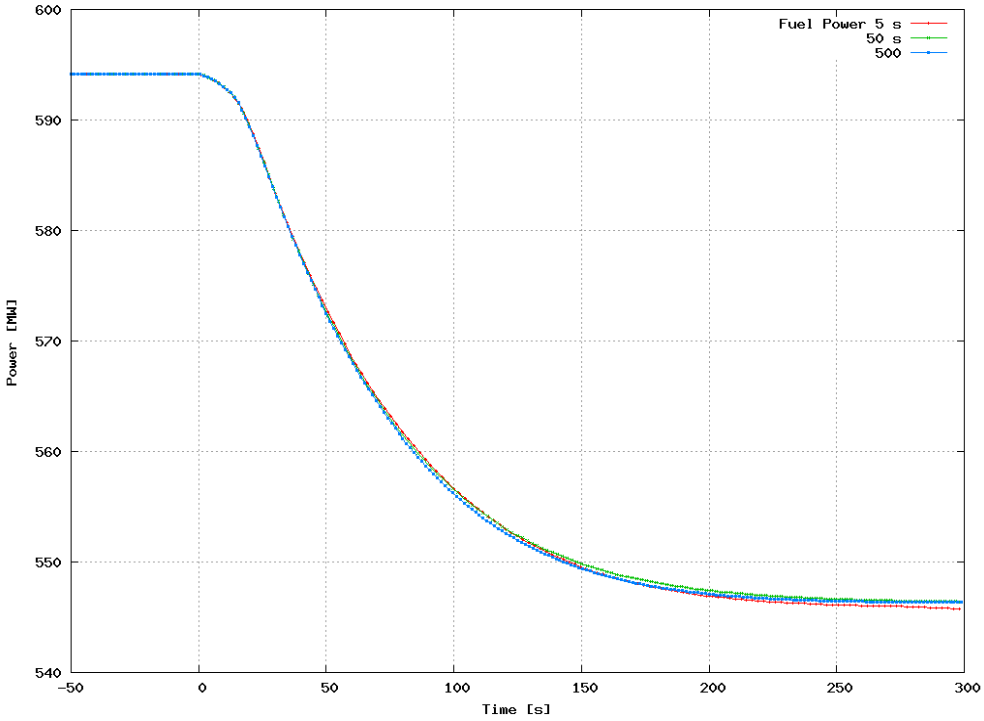


Figure 5-11 Power in Fuel as a Function of Mixing Time Constant

# 6. CONCLUSIONS

Nuclear-hydrogen will need to compete on three fronts: production, operability, and safety to be viable in the energy marketplace of the future. We examined the operability of a nuclear-hydrogen plant while production was examined in [Oh 2007b]. Safety is to be addressed in future work. Plant operability is the degree to which time varying production demands can be met while staying within equipment limits. Criteria for gauging operability were developed and applied to one of the two reference DOE/INL plants for hydrogen production, the Very High Temperature Reactor coupled to the High Temperature Steam Electrolysis process.

The degree of operability inherent in the reference plant was characterized in terms of the underlying physical processes. The description included the role of individual component time constants and energy capacitances and the inherent relationships among process variables including reactivity versus temperature and properties of near-ideal gas coolants. It was shown how each of these phenomena acts to shape operability.

Prior to performing dynamic simulations some simple analytic methods involving component time constants and energy capacitances were used to characterize the dynamic behavior of the VHTR coupled to the HTSE plant. First, the time needed to start up the combined plant based on heat capacity considerations alone and assuming a linear ramp up of reactor power is about four hours. This is less than a typical startup time of 24 hours for a nuclear plant. However, in the analysis there was no consideration given for exceeding limiting thermal stresses. Second, temperature rates of change during a load change were estimated. A ten percent step change in hydrogen production rate would result in a maximum average rate of change in temperature in the hydrogen plant of less than 0.2 C/s before the control system began to re-establish equilibrium with the rest of the combined plant. Given the relatively small size of the components in the HTSE plant and, hence, a small wall and tube sheet thickness, this rate of change does not appear to present a thermal fatigue problem. Third, the failure to thermally isolate the HTSE boiler from the molten salt process heat loop coming from the reactor following a reactor trip and its consequence for the state of the molten salt coolant was investigated. It is important to avoid freezing the salt. It appears that the temperature of the salt might be reduced by as much as 20 C. Given that there might be a couple of hundred degrees margin between the coldest point in the loop and the salt freezing temperature no large-scale freezing appears possible. Whether local freezing occurs would depend on the natural circulation characteristics of the molten salt loop. Fourth, it was found through a study of time constants and energy capacitances that rates of temperature change in the HTSE plant are largely determined by the thermal characteristics of the electrolyzer. It's comparatively large thermal mass and the presence of recuperative heat exchangers result in a tight thermal coupling between the electrolyzer and other HTSE components.

A control strategy for meeting changes in hydrogen demand at the plant fence was developed and evaluated using the GAS-PASS/H dynamic simulation code. It was assumed that the demand for hydrogen can vary from 30 to 100 percent of the full power production rate. The strategy uses inventory control in the VHTR plant and flow control in the HTSE plant to attempt to maintain constant hot side temperatures. Active electrolyzer cell area is varied such that electrolyzer joule heat varies linearly with hydrogen production rate. In an initial simulation

controlled flows were varied linearly with hydrogen production rate. The simulations show that hot side temperatures can likely be maintained near constant. Second order nonlinearities in the HTSE plant will require that each controlled flow be its own non-linear function of hydrogen production rate. A means for determining these flowrates was described and in future work the GAS-PASS/H code will be used to calculate them.

A dynamic simulation confirmed earlier work that suggested thermal transients arising in the chemical plant are strongly damped at the reactor making for a stable combined plant. The large Doppler reactivity component, three times greater than next reactivity component per unit temperature, is mainly responsible. This is the case even for long process heat transport times which create the potential for out-of-phase oscillations in temperature at the reactor inlet and outlet.

It is noted that plant specifications for meeting hydrogen production demand rates at the plant fence will dictate the operational control strategy. Thus, a good understanding of the hydrogen market that the plant will serve is needed. Systems integration studies should in the future attempt to define a set of demand requirements a plant must meet. These would be based on projections for hydrogen demand on a daily, weekly, yearly, and geographic basis; and the role of local storage in mitigating the impact of temporal swings in hydrogen demand on plant operation.

# 7. REFERENCES


Boyack B., et al., *Quantifying Reactor Safety Margins, Application of Code Scaling, Applicability, and Uncertainty Evaluation Methodology to Large-Break, Loss-of-Coolant Accident*, NUREG/CR-5249, Nuclear Regulatory Commission, December 1989.

Carstens N., "Control Studies for Supercritical Carbon Dioxide Power Conversion Systems," Ph.D. thesis, Department of Nuclear Engineering, Massachusetts Institute of Technology, June 2007.

Davis C.B., Oh C.H., Barner R.B., Sherman S.R., and Wilson D.F., Thermal-Hydraulic Analyses of Heat Transfer Fluid Requirements and Characteristics for Coupling a Hydrogen Production Plant to a High-Temperature Nuclear Reactor, INL/EXT-05-00453, June 2006.

Depiante E.V., "Stability Analysis of a Liquid-Metal Reactor and Its Primary Heat Transport System," Nuclear Engineering and Design, 152, pp.261-377, 1994.

Hartvigsen J., personal communication, Ceramatec, November 28, 2006.

Lillo T. M., *et al*., "Engineering Analysis of Intermediate Loop and Process Heat Exchanger Requirements to Include Configuration Analysis and Materials Needs," INL/EXT-05-00690, September 2005.

MacDonald P., NGNP Point Design – Results of the Initial Neutronics and Thermal-Hydraulics Assessments during FY-03, INEEL/EXT-03-00870 Ref. 1, September 2003.

Oh C. H., *et al.*, "HyPEP FY06 Report: Models and Methods," INL/EXT-06-11725, 2006.

Oh C.H., personal communication, Idaho National laboratory, November 2006a.

Oh C.H., Davis C.B., Han J., Barner R., Sherman S., Vilim R., Lee Y., amd Lee W., HyPEP FY06 Report: Models and Methods, INL/EXT-06-11725, September 2006b.

Oh C.H., *et al.,* "Development of GAMMA Code and Evaluation for a Very High Temperature Gas-Cooled Reactor," 2007 International Topical Meeting on Safety and Technology of Nuclear Hydrogen Production, Control, and Management," Boston, Massachusetts, June 2007

Oh C.H., Kim E.S., Sherman S.R., and Vilim R.B., HyPEP FY-07 Report: System Model Integration Model Development, INL/EXT-07-12470, April 2007a.

Oh C.H., Kim E.S., Sherman S.R., Vilim R.B., Lee. Y.J. and Lee W.J., HyPEP FY-07 Annual Report: A Hydrogen Production Plant Efficiency Calculation Program, INL/EXT-07-13078, September 2007b.

Ohta T., Solar-Hydrogen Energy Systems, Pergamon Press, 1979.

Patankar S. V., “Numerical Heat Transfer and Fluid Flow,” Hemisphere Publishing, 1980.

Pradhan S., *et al*., Effects of Electrical Feedbacks on Planar Solid-Oxide Fuel Cells, ASME Transactions on Fuel Cell Science and Technologies, vol. 3, issue 4, November 2006.
Shenoy A., Gas Turbine-Modular Helium Reactor (GT-MHR) Conceptual Design Report, Report number 910720/1, General Atomics, July 1996.

Stoots C.M., Engineering Process Model for High-Temperature Electrolysis System Performance Evaluation, Idaho National Laboratory, June 2005.

Vilim R. B., “Transient Response of a Natural Circulating Liquid-Metal Reactor from Time Constants and Energy Capacitances,” Monitoring and Control Technologies for the Secure, Transportable, Autonomous Reactor (STAR), Nuclear Energy Research Initiative Field Work Proposal 24441, September 2001.

Vilim R.B., Cahalan J., and Mertyurek U., GAS-PASS/H: A Simulation Code for Gas Reactor Plant Systems, ICAPP 2004, Pittsburgh, PA, June 2004.

Vilim R.B., Argonne National Laboratory, private communication, October 2006.

Vilim R.B., “Dynamic Modeling Efforts for System Interface”, ANL-07/16, Argonne National Laboratory, December 2006a.ANL-07/16,

Vilim R.B., “Power Requirements at the VHTR/HTE Interface for Hydrogen Production,” Proceedings of ICAPP 2007 Nice, France, May 13-18, 2007.

Vilim R.B., “GAS-NET:  A Two-Dimensional Network Code for Prediction of Core Flow and Temperature Distribution in the Prismatic Gas Reactor,” ICAPP 2007 International Congress on Advances in Nuclear Power, Nice, France, May 13-18, 2007a.


**Nuclear Engineering Division**
Argonne National Laboratory
9700 South Cass Avenue, Bldg. 208
Argonne, IL 60439-4842

www.anl.gov

UChicago ▶ Argonne LLC

A U.S. Department of Energy laboratory
managed by UChicago Argonne, LLC